



HAL
open science

Northwest Africa 5790: Revisiting Nakhlite Petrogenesis

Albert Jambon, V. Sautter, Jean-Alix J-A Barrat, J. Gattacceca, P. Rochette,
Omar Boudouma, Dominique Badia, Bertrand Devouard

► To cite this version:

Albert Jambon, V. Sautter, Jean-Alix J-A Barrat, J. Gattacceca, P. Rochette, et al.. Northwest Africa 5790: Revisiting Nakhlite Petrogenesis. *Geochimica et Cosmochimica Acta*, 2016, 190, pp.191-212. 10.1016/j.gca.2016.06.032 . hal-01346246

HAL Id: hal-01346246

<https://hal.sorbonne-universite.fr/hal-01346246v1>

Submitted on 18 Jul 2016

HAL is a multi-disciplinary open access archive for the deposit and dissemination of scientific research documents, whether they are published or not. The documents may come from teaching and research institutions in France or abroad, or from public or private research centers.

L'archive ouverte pluridisciplinaire **HAL**, est destinée au dépôt et à la diffusion de documents scientifiques de niveau recherche, publiés ou non, émanant des établissements d'enseignement et de recherche français ou étrangers, des laboratoires publics ou privés.

**Northwest Africa 5790:
Revisiting Nakhlite Petrogenesis.**

A. Jambon*^{1, 4}, V. Sautter², J-A Barrat³, J. Gattacceca⁵, P. Rochette⁵, O. Boudouma^{1, 4}, D. Badia^{1, 4}, B. Devouard^{5, 6}

¹: Sorbonne Universités, UPMC Univ Paris 06, UMR 7193, Institut des Sciences de la Terre Paris (iSTeP), F-75005 Paris, France. albert.jambon@upmc.fr

²: Muséum National d'Histoire Naturelle and UPMC Univ Paris 06, IMPMC, UMR7590 75005 Paris, France. vsautter@mnhn.fr

³: Université de Brest, CNRS UMR 6538 (Domaines Océaniques), I.U.E.M., Place Nicolas Copernic, 29280 Plouzané, France. barrat@univ-brest.fr

⁴: CNRS, UMR 7193, Institut des Sciences de la Terre Paris (iSTeP), F-75005 Paris, France

⁵: Aix-Marseille Université, CNRS, CEREGE UM 34, F-13545 Aix-en-Provence cedex 4, France. gattacceca@cerge.fr

⁶: Université Blaise Pascal, CNRS, Laboratoire Magmas et Volcans UMR 6524, 5 rue Kessler, F-63000 Clermont-Ferrand, France

* Corresponding author

ABSTRACT

Northwest Africa 5790, the latest nakhlite find, is composed of 58 vol. % augite, 6 % olivine and 36 % vitrophyric intercumulus material. Its petrology is comparable to previously discovered nakhlites but with key differences: (1) Augite cores display an unusual zoning between Mg# 54 and 60; (2) Olivine macrocrysts have a primary Fe-rich core composition (Mg#= 35); (3) the modal proportion of mesostasis is the highest ever described in a nakhlite; (4) It is the most magnetite-rich nakhlite, together with MIL 03346, and exhibits the least anisotropic fabric. Complex primary zoning in cumulus augite indicates resorption due to complex processes such as remobilization of former cumulates in a new magma batch. Textural relationships indicate unambiguously that olivine was growing around resorbed augite, and that olivine growth was continuous while pyroxene growth resumed at a final stage. Olivine core compositions (Mg#= 35) are out of equilibrium with the augite core compositions (Mg# 60-63) and with the previously inferred nakhlite parental magma (Mg#= 29). The presence of oscillatory zoning in olivine and augite precludes subsolidus diffusion that could have modified olivine compositions. NWA 5790 evidences at least two magma batches before eruption, with the implication that melt in equilibrium with augite cores was never in contact with olivine. Iddingsite is absent.

Accordingly, the previous scenarios for nakhlite petrogenesis must be revised. The first primary parent magmas of nakhlites generated varied augite cumulates at depth (Mg# 66 to 60) as they differentiated to different extents. A subsequent more evolved magma batch entrained accumulated augite crystals to the surface where they were partly resorbed while olivine crystallized. Trace element variations indicate unambiguously that they represent consanguineous but different magma batches. The compositional differences among the various nakhlites suggest a number of successive lava flows. To

account for all observations we propose a petrogenetic model for nakhlites based on several (at least three) thick flows. Although NWA5790 belongs to the very top of one flow, it should come from the lowest flow sampled, based on the lack of iddingsite.

ACCEPTED MANUSCRIPT

1. INTRODUCTION

As of January 2016 there are 162 recorded Martian meteorites, the so-called SNC (S for Shergottites, N for Nakhrites and C for Chassignites), plus a few non-SNC (see Meteoritical Bulletin database). Among those, the nakhrites represent only 7 meteorites (MIL 03346, NWA 817, Y-000593, Nakhla, Governador Valadares, Lafayette and NWA 998); Northwest Africa (NWA) 5790 and pairs thereof. NWA 5790 was found in the Sahara by nomads and purchased in Erfoud (Morocco) in 2010. The seven previously described nakhrites share a number of common features, such as their crystallization and cosmic ray exposure ages (1.3-1.4 Ga and 11 ± 1.5 Ma respectively, Nyquist et al. 2001). They are all olivine-bearing clinopyroxenites with a cumulate texture defined by coarse augite and olivine crystals set in a fine-grained mesostasis. The coarse subhedral crystals suggest a rather slow growth over a relatively long period of time (> 100 y) (Friedman-Lentz et al 1999, Day et al. 2006) within a sub-surface magma chamber while microcrystals in the mesostasis correspond to a faster cooling stage as crystal mushes were extruded to the surface. It is noteworthy that for a lava flow to spread out, the crystal to melt ratio may not exceed 50 %; this implies that nakhrites accumulated phenocrysts after emplacement. The previously studied nakhrites show subtle differences (mesostasis proportions, cumulus crystal compositions and overgrowths, crystallinities of the mesostasis), which allows them to be positioned within a lava pile with some stratigraphic order from MIL 03346, the uppermost part of the pile, down to NWA 998 at the base of the flow (Mikouchi et al 2003, Treiman 2005 and references therein). Crystal settling and increasing compaction throughout the nakhrite pile likely occurred after extrusion (Day et al. 2006). Estimates of the final cooling rate increase from NWA 998 to MIL 03346 and range 1 to 6 °C/hour (Sautter et al. 2002, Hammer and Rutherford 2005).

Thus nakhlites would have cooled at the Martian surface over short periods of time from 8 to 48 days (Day et al. 2006). The discovery of NWA 5790 offers additional information to better constrain the formation of nakhlite in the magma chamber and extrusion conditions onto the surface. In this paper, we present the petrology, mineralogy and geochemistry of NWA 5790, and compare this new find with the other nakhlites to discuss: (1) the crystallization conditions of cumulus augite in the nakhlite magma chamber, (2) the status of olivine in the Nakhlite Parental Magma, and (3) the final position of NWA 5790 within the pile at the Martian surface.

2. ANALYTICAL METHODS

Freshly broken pieces of NWA 5790 were polished to obtain two thick sections **A** and **B** of 0.75 cm² and 0.63 cm² respectively (Fig. 1). Additional broken pieces were preserved for wet chemical analysis.

Microscopic observations and quantitative chemical analyses of the various phases were made on the polished sections of NWA 5790. Backscattered electron (BSE) images were taken with a Zeiss Supra 55 scanning electron microscope (SEM) equipped with an energy dispersive spectrometer (EDS) at UPMC. Chemical maps were performed using a Bruker QUAD EDS detector and software Quantax at 15 kV and 36 nA (about 300 000 cps). Electron microprobe (EMP) analyses were performed with a Cameca SX100 (WDS) at UPMC (CAMPARIS). Operating conditions were: 15 kV accelerating voltage with a probe current of 10 nA, a counting time of 10 s, and a focused beam for all phases but feldspar and glass (defocused at 4 μm). Natural silicates and synthetic oxides were used as standards for all elements: albite (Na); orthoclase (K); diopside (Mg, Si, Ca); anorthite (Al); MnTiO₃ (Mn, Ti); Cr₂O₃ (Cr);

Fe₂O₃ (Fe); NiO (Ni); apatite (P); pyrite (S). Analyses of a reference Atlantic MORB glass (CH98-DR12) and Celessou and San Carlos olivines permit to avoid systematic deviations outside the reported uncertainty (Baghdadi et al., 2015). The analytical reproducibility of the EMP data is 0.5 % relative for Si (olivine, augite) and 1-3 % relative for elements present in excess of 1 wt. %. It is better than 30 % relative for elements on the order of 0.1 %. The composite color picture (Fig. 1 b) is a WDS X-ray map acquired on the CAMECA SX100 electron microprobe at Laboratoire Magmas et Volcans, Blaise Pascal University (France). Analytical conditions were: 20 kV accelerating voltage, 100 nA beam current, 10 µm defocussed beam, and 40 ms dwell time. Raw intensity maps were combined into RGB pictures.

For in-depth analysis of oscillatory zoning in olivine and augite specific procedures were applied as the relative variations from one point to the next were only several times the analytical uncertainty) (see electronic supplement). Chemical oscillations of short wavelength are reported about the mean local value, which permits to show at the same scale, variations of small amplitude from the core and the rim with strongly different compositions. These variations of small amplitude are not visible on BSE images for two reasons: because of the overall much larger compositional variations on one hand and the short scale (a few micrometers). Under specific tuning of the SEM, some oscillatory zoning can be seen on restricted areas (see online supplement). There are several ways of presenting small chemical variations:

- Oxide wt.% as obtained from EMPA. In this case instrumental noise (resulting from polishing, focusing, current instability, etc.) may overcome the chemical signal. This way is often preferred as it avoids error correlation (the sum is not 100%).

- As a.p.f.u. (Atom per formula unit) based on a fixed number of cations.

Doing so we minimize instrumental errors (e.g. current instability is the same for all cations during one single analysis) but we may introduce spurious variations (e.g. Si in olivine will vary simply because of analytical errors on the other cations and *vice versa*). This problem will arise every time a closure condition (i.e. constant sum of cations) is introduced.

- As a.p.f.u. with a free number of cations. This is equivalent to working with oxide wt. % but permits statistical calculations were all cations have the same weight. For instance, a variable Mg/Fe ratio does not change the number of Si atoms. In the case of olivine variations in Si will result from analytical errors only (P and Al which could substitute for Si are significantly below the analytical error on Si).

We preferred this last way of presenting data, nevertheless all methods should yield the same results if the variations are robust, i.e. outside the error bars (see online supplement). Our preferred method permits verifying that Si is constant in olivine, that the sum (Mg+ Fe) is constant to the first order and (Mg+Fe+Ca+Mn) is constant to the second order. We can therefore introduce statistical tests on the data to assess to what extent these rules are observed, and similarly check whether the variations of Mg (for instance) are outside the error bars. We applied these procedures to reference samples (e.g. San Carlos olivine) and NWA 5790 alike.

The mesostasis of NWA 5790 was analyzed with EMP using a specific procedure. The beam was operated in raster mode with a current of 40 nA, over areas of 250x150 micrometers. According to SEM images, mesostasis is partly crystallized and the composition of the mesostasis from spot analysis is meaningless (no reproducibility); we therefore expected that areas as large as possible would yield an average composition. In order to assess the validity of this assumption 14 areas were

analyzed. The error is estimated from $\sigma/n^{1/2}$, where σ is the standard deviation and n is the number of areas investigated. For the purpose of comparison, we analyzed the mesostasis on a section of MIL 03346 (,123) and a section of NWA 817 under similar conditions. Due to the smaller size of the mesostasis pools in NWA 817, the rastered areas were smaller (100 x 60 micrometers). In order to obtain a similar representative data set for NWA 817, the number of rastered areas was increased to 53. Consistency of the results was checked by analyzing pyroxene and olivine cores using the same procedures in all three sections. Note that low totals are inherent to the procedure: cracks and voids in the mesostasis cannot be avoided in scanning mode; focusing is not perfect because of soft silicates (e.g. glass).

The modal composition has been estimated from pixel counting on BSE images, using 29 images of 3 Mpixels each (magnification x50) and one image of the whole section of 23 Mpixels. For estimating phase abundance in the mesostasis, 9 additional pictures at higher magnification (0.25 mm² each, magnification x200) were considered.

A 500 mg fragment of NWA 5790 was powdered using a boron carbide mortar and pestle. Major elements were determined at the Université de Bretagne Occidentale in Brest (France), by ICP-AES (inductively coupled plasma-atomic emission spectrometry) using the procedure described by Cotten et al. (1995). The accuracy of this system is better than 5 %, and the reproducibility better than 3 %. Trace element concentrations were measured at the Institut Universitaire Européen de la Mer (IUEM), Plouzané (France), by ICP-MS (inductively coupled plasma-mass spectrometry) using a Thermo Element 2 spectrometer following the procedure described by Barrat et al. (2012). Based on standard measurements and sample duplicates, trace element concentration reproducibility is generally better than 5 %,

except for W, which is generally better than 10 %. Two splits were analyzed. Trace element analysis by laser ablation ICP-MS in NWA 5790, MIL 03346 and NWA 817 complements the above set of major elements. The analytical procedures are those described in Barrat et al. (2009).

Magnetic properties of a 1.16 g fragment were studied using standard techniques described in Rochette et al. (2005). These include measurement of magnetic susceptibility, and hysteresis properties. In addition the fabric of NWA 5790 has been investigated through measurement of the anisotropy of magnetic susceptibility (AMS) of the same fragment using standard measurement techniques described in Gattacceca et al. (2008). This technique is non destructive and allows measurement of the three-dimensional fabric on bulk samples. It is representative of the preferred orientation of magnetic minerals (magnetic fabric), which in magmatic rocks is generally representative of the overall rock fabric (Tarling and Hrouda, 1993).

3. RESULTS

3.1. Petrography

NWA 5790 is a medium grained rock with dominant millimeter sized euhedral phenocrysts of augite (0.3-2 mm) (Fig. 1) with length not exceeding 2 mm. A few subhedral olivine phenocrysts with similar size (1-3 mm) are found concentrated at the rim of section *A*, and dispersed in section *B*. A few microphenocrysts of titanomagnetite are also present. The mesostasis is abundant, with typical pocket size on the order of 0.5-3 mm. The mode (vol. %) is as follows: Clinopyroxene 57.8 ± 4 %, mesostasis 36.3 ± 3 %, olivine 5.6 ± 5 %, (barely enough to make it an orthocumulate),

titanomagnetite 0.3 ± 0.2 %, where the statistical error is at the 2-sigma level. The large relative error on olivine abundance results from the presence of only 5 and 9 large phenocrysts in all of sections *A* and *B* respectively. However our olivine mode is within errors of results published previously for the same rock (Tomkinson et al. 2015). The texture of NWA 5790 strongly recalls NWA 817 and MIL 03346 but the abundance of the mesostasis is the highest ever described in a nakhlite.

/Fig. 1. Global BSE Image/

Augite exhibits a thin Fe-enriched rim when in contact with the mesostasis (Fig.1 and 2). This rim thickness is about 10-30 micrometers, depending on crystal orientation with respect to the polished section surface (Fig. 2). Such a rim, already described in other nakhlites, becomes thinner or absent when in contact with other cumulus grains such as olivine, augite or titanomagnetite. In NWA 5790 rims are particularly sharp compared to those in all other nakhlites including NWA 817 (10-50 micrometers) and MIL 03346 (70-100 micrometers). Contrast enhancement shows that most of the augite cumulus crystals exhibit unusual irregular recurrent zoning absent in the other nakhlites (possibly cryptic in NWA 817). They exhibit resorbed cores with an irregular shape overgrown by a less magnesian composition. Rounded augites are included in olivine indicating that its resorption was followed by incorporation in growing olivine before the final overgrowth of augite (Fig. 1B). These fragments exhibit the typical irregular zoning but are devoid of the Fe enriched rim indicating that olivine growth occurred before the last stage of rim pyroxene growth.

The only shock effect observed is mechanical twinning. Augite contains few melt pockets of trapped mesostasis similar to those described in MIL 03346 (Sautter et al 2006).

/Fig. 2 contrasted BSE Image/

Olivine varies in size from macrocrysts (about 2 mm) slightly larger than cumulus augite to smaller grains and appears unevenly distributed in the studied sections. One small anhedral crystal is observed in the center of section A (Fig. 1). Olivine is euhedral when abutting mesostasis and it lacks the dark lamellar symplectite exsolution (augite-magnetite intergrowths) observed in Nakhla and Governador Valadares (Greshake et al 2000; Mikouchi et al. 2000).

Fracturing of pyroxene and olivine is moderate like in other nakhlites and unlike any shergottites. Olivine unlike augite is steadily zoned with a Fe-enriched rim on the order of 50 micrometers similar to what is observed in MIL 03346 and sharper compared to NWA 817 (about 100 micrometers). Neither orthopyroxene nor pigeonite is observed replacing olivine, like in NWA 817 and MIL 03346. One olivine crystal (section B) contains a large magmatic inclusion rich in Cl-amphibole (nearly one third of the inclusion) and apatite similar to those described in MIL 03346 (Sautter et al., 2006). Rare melt inclusions may be present at the rim of augite when included in olivine.

One titanomagnetite euhedral phenocryst is present in section A (Fig. 1B) containing ilmenite exsolution and a significant magmatic inclusion with pigeonite, Na and K feldspar, and apatite.

Thin amphibole films can be found within fractures of augite. Its aspect is different from the iddingsite observed in other nakhlites, as it is clearly not a low temperature alteration product of its host.

Interstitial mesostasis is much more abundant in NWA 5790 than in all the other nakhlites, about 36 vol. % compared to 20 % in MIL 03346, the uppermost nakhlite in the pile until now. Mesostasis contains dendritic cross-shaped oxides, Fe-rich

pyroxene and fayalitic olivine set in a glassy, poorly crystallized, feldspathic and silicic groundmass (Fig. 2). Plagioclase laths as seen in most other nakhlites (Treiman 2005) are lacking, as in MIL 03346. Mesostasis titanomagnetite amounts to 0.6 ± 0.2 vol. %, dendritic chains of iron-rich olivine and pyroxene 3.4 ± 0.8 % and glass, silica and feldspar 31.9 ± 0.9 %. The olivine and pyroxene chains in the mesostasis are about 2-4 μm wide and form a striking rectangular pattern. Submicrometric exsolutions of ilmenite amount to about 10 % of host titanomagnetite. The small size of the phases and the intermediate and variable compositions of glass make it difficult to distinguish accurately between glass, silica, and zoned K-feldspar or albitic plagioclase. One occurrence of chalcopyrite has been observed as in Nakhla (Greenwood et al. 2000).

3.2. The anisotropy of magnetic susceptibility (AMS)

The three-dimensional petrofabric of NWA 5790 was investigated using the anisotropy of magnetic susceptibility (AMS). Previous studies (e.g., Gattacceca et al. 2008) concluded that in basaltic shergottites and nakhlites, AMS might be a proxy of the original magmatic fabric. Here we present AMS data for NWA 5790. We also provide data for other nakhlites that were not studied in Gattacceca et al. (2008): Y-000593, NWA 817, and additional data for MIL 03346.

A synthesis combining these new results together with previous data (Collinson, 1997; Gattacceca et al., 2008) is presented in table 1. The AMS is characterized by P_r , the ratio of maximum to minimum ferromagnetic susceptibility (Gattacceca et al., 2008), and the shape parameter T (Jelinek, 1981) ranging from -1 for prolate fabric (well-developed lineation) to +1 for oblate fabric (well-developed foliation).

/Table 1: Magnetic properties of nakhlites/

The magnetic fabric of nakhlites is oblate (foliated texture) with a mean T of 0.32, which is expected for a cumulate, and in agreement with the observed rock texture and preferred orientation of augite crystals (e.g., McSween, 1994). The degree of anisotropy P_f ranges from 1.005 to 1.040 (average 1.023, standard deviation 0.010) with NWA 5790 having the lowest value at $P_f=1.005$. It is noteworthy that based on petrological criteria, NWA 998 ($P_f=1.031$) and Lafayette ($P_f=1.040$), the most anisotropic samples, have been suggested to be the deepest samples of the nakhlite igneous body, with a burial depth >30 m (Mikouchi et al., 2006). We propose that higher lithostatic load resulted in a more developed magnetic foliation with respect to other nakhlites. Conversely, the very low magnetic anisotropy of NWA 5790 ($P_f=1.005$) may indicate a very shallow origin for this meteorite, shallower than the 1-2 m that is the depth estimated for NWA 817 (Mikouchi et al., 2006).

3.3 Mineralogy

Representative compositions of the most significant phases are reported in tables 2-8

Pyroxene (Table 2, Fig. 3-4)

/ Table 2 Augite analyses/

Augite exhibits unusual core compositions not observed in any of the other nakhlites. In NWA 5790, augites display irregular recurrent zoning mostly due to FeO/MgO variations. Zones of comparatively high Fe alternate with relatively Fe-poor zone with irregular boundaries (Mg# varies between 0.54 and 0.63, $En_{35-38}Fs_{25-22}Wo_{40}$ and Fe/Mn = 40-32). Irregularity of zoning can be observed in BSE images: in Figure 2, ghost augite rich in Mg (dark grey) with variable composition (Mg# 61-58) and with irregular boundary is surrounded by augite poorer in Mg (light grey, Mg# 55-50). The

outermost rim enriched in Fe (white) against the mesostasis may be absent. In the same crystal the transition from Mg rich core to the less Mg rich overgrowth may be either discontinuous or steady depending on which part of the crystal is concerned. EMP traverses performed across augite crystals (Fig. 3) show that Al, Ti, Cr and Mn anticorrelate with Mg#. Ca and Na remain nearly constant (Table 2). These heterogeneous cores are surrounded by rims of hedenbergite composition up to $\text{En}_{20}\text{Fs}_{43}\text{Wo}_{36}$ (and Fe/Mn = 45-40 for Mg# =20-50) (Fig. 3). Ca decreases and increases again at the very rim only slightly. A similar, though more marked feature has been observed in MIL 03346 exclusively, whilst in other nakhlites as Fe increases Ca decreases as well, giving rise to a pigeonitic rim. In NWA 5790 the Al_2O_3 content increases to 4 wt. % towards the rim as the Mg# decreases from 0.6 to 0.2; the TiO_2 content exhibits a similar trend, with low 0.2 to 0.6 wt. % in the core and enrichment up to 1.6 wt. % at the rim of Mg# 0.2. In contrast to Al and Ti, the Cr_2O_3 content decreases from 0.38 wt. % down to below detection. The overall composition of augite can be visualized in the conventional pyroxene quadrilateral (Fig. 4) and compared to augite compositions in MIL 03346.

/Fig. 3 Cpx Ol zoning/

/ Fig. 4 Cpx quadrilateral/

Superimposed on the overall zoning, EMP analyses reveal a faint oscillatory zoning for major and minor elements, including the Mg#, Si, Mg, Ca, Fe, Al with a wavelength on the order of 15 μm , from the core to the rim (Fig. 5a). The oscillations are for atoms per formula unit (p.f.u.) (See on line supplement). The wavelength observed is independent of the sampling step, which was varied by a factor 10. One wave always corresponds to several data points (sampling step down to 1 micrometers) and several waves are observed. The same will be shown for olivine

(see below) though at a different wavelength. Therefore cyclic variations of the background noise cannot be responsible for such oscillations.

Despite a similar wavelength, no simple correlation is observed between the various elemental variations. The amplitude of oscillatory zoning is too small to be visible on BSE images. Oscillatory zoning in lavas is usually interpreted as the result of disequilibrium due to rapid growth. MIL 03346 is the only nakhlite where oscillatory zoning restricted to rim pyroxene was previously noted (Anand et al. 2005).

In the mesostasis of NWA 5790, acicular intercumulus pyroxene is Fe-enriched with variable composition (about $\text{En}_{11}\text{Fs}_{49}\text{Wo}_{34}\text{Ku}_4\text{Ti-Tsch}_1$ and $\text{FeO/MnO} = 46$). It is enriched in aluminum (Tschermak components).

Olivine (Table 3)

/Table 3 olivine analyses/

Olivine cores are homogeneous and exhibit the same composition from one crystal to the next, $\text{Fa}_{65.5 \pm 0.5}$ with $\text{Fe/Mn} = 47 \pm 3$ ($n = 142$). The rim with a thickness on the order of 50 micrometers is zoned from Fa_{65} to Fa_{90} with increasing Fe/Mn to 40 (Fig. 3).

This rim is quite thin, being a factor of 10 smaller than the crystal radius (more than 500 μm). Clearly the primary olivine core composition is preserved and is not affected by possible late exchange with the melt.

Interestingly, this core composition is more fayalitic than those preserved in olivine from MIL 03346, NWA 817, and Y-000593, the uppermost rocks of the nakhlite pile, and similar to that of NWA 998 ($\text{Mg}\# = 0.35$). The small interstitial olivine crystals of the mesostasis are fayalitic and show the same composition as the megacryst rim ($\text{Mg}\# = 6$). The most ferroan composition of olivine in the mesostasis is Fa_{93} .

At first sight, the CaO content in olivine megacrysts does not show significant variations and remains between 0.5 and 0.6 wt. %. However EMP analyses reveal Ca, Mn, Mg and Fe oscillatory zoning with a wavelength of about 3 micrometers similar to what is observed in pyroxene (Fig. 5b) (see on line supplement). In figure 5b we present the variations of Mg about a local average (long range filtering; see on-line supplement) as it permits to include the variations of the rim.

Oscillations are present in both core and rim of olivine. Detailed description of oscillatory zoning is beyond the scope of this paper; still, as will be seen below this result has far reaching implications and therefore deserves an in-depth presentation (see also on line supplement). The most important point at this stage is to prove that the observed variations are real and not due to background noise. The case of olivine is the easiest for the purpose of the demonstration. From the structural formula of olivine $(\text{Mg, Fe})_2 \text{SiO}_4$ we expect that, when expressed on a molar basis, Si and (Mg+Fe) should be constant. From careful chemical analyses we know that the contributions of Al and P, which could substitute for Si, are less than the analytical error (one sigma) for Si. Therefore Si should be constant within analytical errors, which is what is observed. For (Mg+Fe) we observe some substitution by Ca and Mn which are not negligible but represent less than 3 % of the (Mg+Fe) total. Therefore we can neglect this contribution in the following discussion. A statistical analysis of the results indicates that the variations of Mg and Fe are negatively correlated which cannot be explained by random analytical errors (counting statistics) or systematic errors (which would imply a positive correlation).

This result is important as it means that chemical diffusion in olivine was negligible as it would have erased these short wavelength variations; zoning at the rims of phenocrysts must result from the closed system evolution of melt composition and olivine overgrowth, not from diffusional exchange with the melt (subsolidus or not).

/Fig. 5 Augite + Olivine oscillatory zoning/

Mesostasis

Mesostasis is dominated by either plagioclase ($An_{20}Ab_{72}Or_8$ on average) or K-feldspar ($An_{13}Ab_{25}Or_{65}$ on the average) compositions which exhibit significant variability (Table 4) with silica and glassy silica-rich compositions. Crystallinity is variable, with some mesostasis pools containing a significant fraction of silica-feldspathic glass (Fig. 6). Note that all phases in the mesostasis, including olivine, augite, plagioclase, silica and oxides exhibit low EMP totals. This is because of the small size and/or dendritic aspect of the phases.

/ Fig 6 : BSE image of mesostasis/

The average compositions of 12 mesostasis pockets have been measured in scanning mode, which permits the determination of an average mesostasis composition including all dendritic crystals. Results are reported in Table 5 and compared with the mesostasis

/(Table 4 mesostasis silicates/

/Table 5 mesostases) /

compositions of MIL 03346 and NWA 817 measured using a similar procedure.

The first interesting feature is the close similarity of the mesostases in all three nakhlites. According to the different thickness of overgrowths of augite and olivine in the different rocks, we did expect that mesostasis composition would be affected in proportion to the respective fractions of mesostasis and overgrowth. As this is not the case, we must conclude that overgrowths predate some compaction of the melt included in intercumulus pools, and that the amount of presently observed mesostasis represents the same final melt evolution and not a variable intracumulus evolution.

Alteration products

The product of olivine, augite and mesostasis alteration as found in most other nakhlites (iddingsite/smectite) (Gillet et al. 2002; see also Treiman 2005 and references therein) is absent in NWA 5790 (Tomkinson et al. 2015). Instead we find in some augite and olivine fractures, in a different textural setting, a product of unspecified mineralogy, which we infer to be a mixture of amphibole and smectite of variable composition (Fig. 7; Table 6). The low totals may be due to the microcrystalline and/or hydrous nature of the phases. One type is low in Al and high in Ca and Fe with a rather high Mg# (27 - 59); it is neither olivine nor smectite. The second is high in Al, Na and K, lower in Ca, Fe and Mg. Its low Mg# (7 to 20) suggests a late (possibly hydrothermal) crystallization. Both types contain variable amounts of Cl from 0 to 3 wt. %. A plot of Cl against Al (not shown) reveals the existence of a chlorine rich type in addition to the low- and high-Al types already mentioned; interestingly the composition of this type is similar to the amphibole described by Sautter et al. (2006) in MIL 03346. The average composition of the Cl rich compositions is displayed in Table 6 suggesting that it likely is a mixture with dominant amphibole. Subtraction of the Al-rich component from the Cl-rich composition yields a composition similar to the amphibole of MIL 03346.

/Fig 7: BSE image of alteration products /

/Table 6: Amphibole compositions/

Additional minor phases and magmatic inclusions are described in the on line supplement.

Oxides (Table 7)

/Table 7 oxide analyses/

Rare Ti-magnetite phenocrysts $Uv_{32}Mt_{56}Sp_7Ct_4$ (a solid solution of ulvöspinel, magnetite, spinel and chromite) show fine ilmenite exsolutions, too small to be analyzed accurately with EMP. The fraction of Fe^{3+} , calculated after stoichiometry, is significant with $Fe^{3+}/(Fe^{3+}+Fe^{2+}) = 0.47 \pm 0.01$. They differ from dendritic microcrysts in the mesostasis pockets which exhibit a wider compositional range: $Uv_{52-74}Mt_{38-19}Sp_{2-1}$ (see Table 7), $Fe^{3+}/(Fe^{3+}+Fe^{2+}) = 0.33-0.18$, and contain more Ti, and are Al and Cr free. The high Fe^{3+} fraction partly explains the low totals of table 7. In the mesostasis the crystals are dendritic (Fig. 6) which represents another analytical difficulty contributing to the low totals. Still the calculated structural formulae provide a satisfactory stoichiometry.

Rock magnetic properties of nakhlites: The mineralogy of magnetic minerals of rocks can be studied by magnetic measurements. Magnetic properties of SNC meteorites, apart from NWA 5790, have been reviewed by Rochette et al. (2005). We provide here the magnetic properties for NWA 5790. Low-field magnetic susceptibility (that represents the contribution of ferro-, para-, and diamagnetic minerals) is $\chi = 6.48 \cdot 10^{-6} \text{ m}^3 \cdot \text{kg}^{-1}$, the high-field susceptibility (that represents the contribution of para- and diamagnetic minerals only) is $\chi_{hf} = 4.02 \cdot 10^{-7} \text{ m}^3 \cdot \text{kg}^{-1}$. Saturation remanence is $M_{rs} = 297 \text{ mAm}^2 \cdot \text{kg}^{-1}$, saturation magnetization is $M_s = 1.19 \text{ Am}^2 \cdot \text{kg}^{-1}$, coercivity is $B_c = 32 \text{ mT}$, coercivity of remanence is $B_{cr} = 58 \text{ mT}$. M_s corresponds to 1.3 wt. % of pure magnetite (or more if impure). Magnetite as

microphenocrysts is not abundant (about 0.3 vol. %) which suggest that Ti-magnetite in the mesostasis was underestimated by modal estimation.

3.4. Bulk Rock Geochemistry

Major and trace element analyses were measured on separate splits and are reported in Table 8. To enable an easier comparison with other nakhlites, analyses of NWA 817 (Sautter et al. 2002), MIL 03346 (this work) and Nakhla (Nakamura et al. 1982) are also reported. Key element ratios, which are identical to those measured in other nakhlites, confirm unambiguously the Martian origin ($\text{FeO}^*/\text{MnO} = 38$, $\text{Na}_2\text{O}/\text{Al}_2\text{O}_3 = 0.39$, $\text{K}/\text{La} = 476$, $\text{Ga}/\text{Al} = 3.5 \cdot 10^{-4}$). Bulk major element chemistry reflects the abundance of mesostasis: it is somewhat poorer in Mg and Fe and is richer in Na, K, and Al compared to the other nakhlites: $\text{MgO} = 8.0 \%$ and $\text{Al}_2\text{O}_3 = 5.3 \%$ instead of 11.8% and 1.6% for Nakhla. Otherwise NWA 5790 appears chemically similar to MIL 03346.

/Table 8 Bulk rock major and trace element analysis/

The REE (Rare Earth Element) pattern (Fig. 8A) is characterized by a strong light REE enrichment: $(\text{La}/\text{Yb})_n = 5.5$, and a minor negative Eu anomaly $\text{Eu}/\text{Eu}^* = 0.86$.

NWA 5790 displays the highest Th, U (Fig. 8B) and REE abundances (Fig. 8A) ever reported for a nakhlite (e.g., $\text{Th} = 0.85 \text{ ppm}$).

Weathered finds from the Sahara generally exhibit marked Ba enrichments that are sensitive indicators of the development of terrestrial secondary phases (e.g., Barrat et al., 2003). The high Ba value (285 ppm) and Ba/Rb ratio (39) compared to MIL 03346 (57 ppm and 13) (Fig. 8B) (Day et al. 2006) are strong arguments supporting

contamination for this element. Other analyzed trace elements however do not exhibit detectable enrichment due to this effect. One interesting characteristics of NWA 5790 and other nakhlites as well, is illustrated in an Sr vs Al_2O_3 plot (Fig. 9). The ratio of Sr to Al_2O_3 is high due to the low Al_2O_3 content, especially when compared with shergottites and CI Chondrite. A simple interpretation of this feature is melting at high pressure for the source of nakhlites or melting of an Al depleted source, the Al depletion being in both cases the signature of melting with residual garnet. The difference between these two possibilities could be resolved using Nd isotopic data.

/Fig. 8 REE pattern/spider diagram/

/Fig. 9 Sr vs Al_2O_3 /

LA-ICP-MS analyses of pyroxene, mesostasis and olivine of NWA 5790 are compared to similar analyses in NWA 817 and MIL 03346 (Table 8; Fig. 10). The mesostasis of NWA 5790 contains a high incompatible element abundance like either NWA 817 or MIL 03346 as illustrated by the REE patterns. Variable concentrations (a factor of 2) but identical patterns can be observed in augite. There is no obvious relationship between REE abundance and position in the crystal but the Fe-enriched rims are too thin to be analyzed.

/Table 9 Trace element of separate minerals/

/Fig. 10 REE in phases/

REE in augite

The average REE patterns in NWA 5790, NWA 817 and MIL 03346 are very close to one another with abundances increasing from MIL to NWA 5790 (Fig. 10). When looking more closely at the different patterns however, subtle differences appear. The abundances among the different data points in one single section are quite variable: on

the average the abundances increase by 1.72, 1.69 and 1.29 in MIL, NWA 5790, and NWA 817 respectively but this effect is slightly more pronounced for La, the most incompatible element which increases by a factor of about 2 in all three samples. This should however be considered with care since the number of analytical points is limited and may not document the whole range in each sample. At the same time the Ce/Yb ratio among the different data points increases by 18 % (NWA 5790), 36 % (MIL), 57 % (NWA 817): the pattern is nearly similar (NWA 5790) to slightly fractionated (NWA 817) as the composition evolves. The concentrations in all pyroxenes analyzed exceed those recorded in Nakhla augite by Nakamura et al. (1982). As the augite composition reflects the composition of the melt it crystallizes from, one should conclude that the melt changed composition significantly. The spatial resolution does not permit to decide whether this is a continuous process (e.g. fractional crystallization) (Day et al. 2006, Wadhwa and Borg 2006) or a discontinuous one (magma mixing) or both.

REE in olivine.

The REE patterns in olivine are different in NWA 817, MIL 03346 and NWA 5790 (Fig.10). The two olivines analyzed in NWA 817 differ in their Light REE abundances. If we consider the REE pattern in the smectite of NWA 817 (Gillet et al., 2002), O11 (enriched in light REE) can be derived from O12 with the addition of about 3-5 % of smectite, the exact amount depending on the variable composition of the smectite. The HREE pattern is likely to result from olivine composition (not smectite) as it is similar in the two olivines analyzed, whereas the LREE pattern results from variable amounts of smectites trapped in olivine, a conclusion similar to that obtained by Wadhwa and Borg (2006). The HREE of olivine in NWA 5790 are undistinguishable from NWA 817 whereas the LREE are significantly lower. This

implies the absence of smectite in NWA 5790 olivine, which would increase the abundance of LREE. Finally in MIL 03346 neither the LREE nor the HREE match those of NWA 5790 olivine, except for Lu and Yb. Our results are quite similar to those reported by Day et al. (2006). Nevertheless the pattern is enigmatic and the contribution of smectite is not supported by the data of Gillet et al. (2002). Although the results for smectite in MIL are not available, a very odd composition of smectite would be required in order to obtain the pattern of MIL olivine (Stopar et al., 2013). In other words the REE pattern in olivine most likely reflects the magmatic history in NWA 5790, smectite incorporation in NWA 817, and contamination by smectite or other phases in MIL 03346.

4. DISCUSSION

Like all the other nakhlites, NWA 5790 exhibits a typical cumulate texture, which is reflected in its chemical composition. Phenocrysts of olivine and augite settled down and trapped some intercumulus liquid. NWA 5790 resembles quite closely MIL 03346: it exhibits the same large crystal size, large amount of Ti-magnetite, high mesostasis fraction made of glass and skeletal Fe-augite, Fe-olivine and Ti-magnetite, and lack of plagioclase laths. According to its even higher mesostasis fraction and lower anisotropy, NWA 5790 can therefore be viewed as the uppermost part of the nakhlite lava flow (Mikouchi et al., 2003). Launch pairing with the other nakhlites is likely based on the 9.6 Ma cosmogenic age determined for NWA 5790 (Huber et al. (2012).

This new nakhlite, however, displays at least four specific features that may shed new light on nakhlite petrogenesis: 1) cumulate clinopyroxene complex zoning; 2) olivine

core composition; 3) mesostasis proportion; 4) lack of secondary low temperature alteration. As no iddingsite occurs in the sections studied we will focus exclusively on the three magmatic features mentioned above.

4.1 Augite zoning

4.1.1 *Recurrent internal zoning*

Augite core compositions in NWA 5790, compared to all the other nakhlites, suggest a somewhat different petrogenesis or different cooling conditions before extrusion as a thick lava flow onto the Martian surface. Core augite relates to an early stage of crystallization within a magma chamber (core 1 in Fig. 3 and Table 2). The presence of numerous glomerocrysts indicates that augites were accumulated before their final stage of growth. When enclosed in olivine augite grains are rounded, indicating that they suffered significant resorption before being overgrown, a conclusion supported by their unusual zoning. The Fe-enriched rims are observed in several nakhlites whilst the internal recurrent zoning is described for the first time and corresponds to an early phenomenon not observed elsewhere in the pile. Discontinuous zoning evidences one stage of augite resorption and rounded augite enclosed in olivine corresponds to cores of such crystals without the overgrowth. Transient chemical disequilibrium between the early cumulus phenocrysts and the final liquid composition in the chamber may account for partial augite resorption. Still, despite a moderate compositional difference between the new melt batch and the former one (as recorded in the overall compositions or the two parts of the cores) augite was significantly and irregularly resorbed. This implies at least two stages of growth with some resorption in-between. The second stage permitted the recovery of euhedral shapes. The overgrown core (core 2 in Fig. 3 and Table 2) is depleted in MgO relative to the previous core, indicating that the new melt batch had a lower Mg#. Treiman (2005) suggested for

other nakhlites that a slight Mg# depression in the Mg-rich cores could result from hollow core crystallization. A similar depression in the Mg-rich part of the augite (core 1 in Fig. 3) probably corresponds to that case. Infilling and overgrowing hopper crystals would be a good way to make patchy zoning but this would not produce the rounded crystals included in olivine. If this scenario applied to the other nakhlites, one should distinguish between a rim significantly enriched in iron corresponding to intercumulus growth and an overgrowth surrounding a core of irregular shape. This scheme is clearly visible in NWA 5790 and also in Nakhla (e.g. Goodrich et al. 2013, their Fig. 11) but may not be present in all nakhlites: For example McKay et al. (2006; their Fig. 1) observed a difference between MIL 03346 and Y-000593 based on Al maps: augite cores in MIL appear homogeneous while Y-000593 looks similar to NWA 5790.

The survival of core zoning (Fig. 2) indicates that clinopyroxenes in NWA 5790 were stored where cooling was fast enough to preclude diffusive homogenization. This feature contrasts with the absence of discontinuous zoning in the augite cores of some of the other nakhlites (e.g. MIL 03346).

The composition of augite cores is marginally variable for five nakhlites (Nakhla, Governador Valadares, Lafayette, Y-000593 and MIL 03346) with a narrow range in Mg# from 62.5 to 62.9 respectively, suggesting a common parent melt. For the others (NWA 998, NWA 817 and NWA 5790) the compositions depart significantly with Mg# of 64.5, 66.5 and 60 respectively. As previously suggested (Treiman, 2005) this supports the idea that the melt parent to the augites was not unique, but may correspond to different stages of evolution of one single parent melt.

A more serious difficulty is whether olivine and augite in one single specimen derive from the same parent melt. In the case of NWA 5790 it is quite clear that olivine and augite cores are not in equilibrium suggesting that one at least is xenocrystic. For the

other nakhlites if we consider that the experimental results of Toplis and Carroll (1995) are relevant, none of them appear to be at equilibrium, with MIL 03346 and Y-000593 departing least from equilibrium (Fig. 11). Augite overgrowths on the other /Fig. 11 olivine and augite compositions compared / hand appear to be in equilibrium with olivine (see, e.g., the analyses of augite and olivine in contact with one another in NWA 817 by Sautter et al. (2002)). In the case of NWA 5790, the resorbed habit of augite and its inclusion in olivine indicates that olivine postdates augite. Rounded augites included in olivines can be found in other nakhlites as well. The case is quite clear in NWA 817 and Nakhla (e.g. Fig. 4 in Treiman et al. 2005) indicating that in at least three of the nakhlites both composition and textural relationship indicate that augite is xenocrystic. In the other nakhlites there is no evidence that the same does not apply. The only exception might be MIL 03346 where the augite appears unzoned (except for intercumulus overgrowth) and close to equilibrium with olivine. The case of Y-000593 however where olivine and augite appear close to equilibrium is different: McKay et al., (2006; their Fig. 1) showed that augite cores exhibit resorption zoning and must therefore be considered as xenocrystic

4.1.2. Rim Zoning.

The final rim of augite crystals was produced by crystallization from the final batch of melt after crystallization of core olivine and in chemical continuity with augite overgrowths (Fig. 3). The cores grew from an “infinite” reservoir whereas the rims most probably correspond to growth in reservoir of limited size (compared to the crystals), most likely the intercumulus liquid. The strong FeO enrichment of the rim may partly reflect some disequilibrium growth due to strong undercooling. From the

mesostasis FeO/MgO of 29 and the K_D value of 0.18 (Toplis and Carroll, 1995) one should expect a $(\text{FeO/MgO})_{\text{Aug}}$ of about 5 compared to the observed value of 8 at the very rim. This is exactly what is expected from a compositional gradient at the melt-crystal interface at rapid growth rate when diffusive transfer is limited in the melt. The out-of-equilibrium composition of augite rim is another hint that the compositional gradient at the augite rim is not due to diffusive exchange in the crystal but to the evolution of the melt. We also note that the absence of diffusive exchange in the crystal is supported by the preservation of core zoning (despite a longer time to equilibrate) and the presence of oscillatory zoning at a wavelength of about 10 micrometers.

4.1.3 Augite oscillatory zoning.

Superimposed on the large wavelength zoning (core and rim) we observe small amplitude compositional variations with a wavelength of about 10-15 micrometers. This results from the coupling of diffusion and growth and is typical of rapid out-of-equilibrium growth (see, e.g., Allègre et al. 1981). Interestingly this suggests fast augite growth as well as sufficiently fast cooling conditions after crystallization to preclude diffusion and thus preserve the compositional variations. Our result is in qualitative agreement with the conclusions of Hammer and Rutherford (2005) and Day et al. (2006) who derived fast cooling rates for MIL 03346 of 3-6°C/hr.

Theoretically, the wavelength of oscillatory zoning is scaled by the ratio D/V , where D is the diffusivity in the melt and V the growth rate. The diffusions of all elements should be coupled since major and minor elements exhibit identical wavelengths. For a temperature of 1080°C, a diffusivity of about $2 \times 10^{-13} \text{ m}^2/\text{s}$ can be inferred (Zhang, 1993) hence a large growth rate on the order of $1.3 \times 10^{-8} \text{ m/s}$, can be calculated.

Accordingly, it would take about five hours for 0.5 mm augite crystals to grow under these conditions. Note that the wavelength is not accurately defined as it may slightly vary along a single profile: D and V depend on the composition at the interface and on its variations to the second order. The wavelength may also vary from one crystal to the next due to various orientations of the profiles. The orientation effect is however small (a factor of <2 at worst) on crystal sections with an aspect ratio significantly different from unity, while the growth estimates are within one order of magnitude.

4.2 Olivine zoning

4.2.1. Olivine bulk zoning

Olivine cores in NWA 5790 are not in equilibrium with augite cores, to an even larger extent when compared to the other rapidly cooled samples from the pile such as MIL 03346 and NWA 817. Using the experimentally based correlation between the Mg# of coexisting liquid, augite and olivine with decreasing temperature (Fig. 12) derived from the experimental results of Toplis and Carroll (1995), a Mg# of 58 in augite should be in equilibrium with a Mg# of 20 in liquid and a Mg# of 40 in olivine at a temperature of 1092 °C (Treiman 1986-93, Longhi and Pan 1989; Harvey and McSween 1992 a-b).

/ Fig. 12 :Olivine/Augite/melt equilibrium/

Therefore olivine of Mg# 35 is out of equilibrium with any melt that precipitated augite cores. Given the textural relationship between olivine and augite (resorbed

augite is included in olivine) the addition of augite from some external source to the nakhlite parental melt (with or without olivine) is mandatory. Olivine however should be in equilibrium with the augite overgrowth. This feature has already been noticed for other nakhlites (Berkley et al., 1980; Nakamura et al., 1982; Treiman, 1986; Longhi and Pan, 1989; Harvey and McSween 1992 b; Sautter et al. 2002).

Olivine core compositions (Mg#= 35) in NWA 5790 are among the most iron rich compositions recorded in nakhlite olivine cores and is close to the composition of 34.8 and 33.9 observed in Governador Valadares and Lafayette (Fig. 4). The composition of the augite cores being totally different confirm, that augite and olivine cores cannot be in equilibrium in at least one of these rocks.

The rim thickness in olivine megacrysts (about 50 μm) is 5 to 20 times smaller than crystal radius (0.2 to 1 mm). According to the sharp rim of olivine in NWA 5790, the observation by Treiman (2005) that “*in general, the highest the Mg# of olivine core, the sharpest the Mg zoning in the rim*” seems fortuitous. The growth of olivine from the melt must have been significant in order to include zoned pyroxene. In other words, the final melt is not parental to the augite cores but it should be the parent of olivine, and the augite overgrowths (Olivine Mg#35, Cpx-overgrowth Mg#50 and mesostasis Mg# 0.16; Fig. 12). This is probably the case for all nakhlites as shown in Fig. 11, where olivine and augite core compositions are plotted: some data points fall close to the equilibrium line, but most of them depart significantly therefrom.

In order to explain the disequilibrium between olivine and augite cores already observed in other nakhlites, one hypothesis, strongly suggests that olivine composition results from diffusive re-

equilibration between olivine and late-stage interstitial melt or subsolidus equilibration with the mesostasis (e.g., Longhi and Pan, 1989; Harvey and McSween 1992a, Mikouchi et al. 2003 and Sautter et al. 2002). As already noticed in NWA 817 (Sautter et al. 2002), the progressively truncated zoning of olivine when in contact with augite precludes subsolidus diffusion: This feature indicates that zoning formed while both olivine and augite were still growing one against the other. In the case of NWA 5790 this explanation is impossible at least from obvious textural evidence (olivine core composition is primary as the “characteristic diffusion length” (= rim thickness) of 50 μm (Fig. 3) is significantly smaller than the crystal radius of 400–500 μm).

As expected however, the augite overgrowth and olivine when in contact with each other are equilibrated. Moreover, rare melt inclusions trapped in-between are also in equilibrium (Fig. 12).

4.2.2. Olivine oscillatory zoning

Subsolidus exchange is not supported by our observations. i) If the olivine rim composition resulted from diffusive exchange, then we should observe a steady profile, with an equilibrium composition at the crystal melt interface: from a mesostasis FeO/MgO of 28.8, a $(\text{FeO}/\text{MgO})_{\text{OI}}$ should be 8.6 compared to the actual value of 13. ii) Oscillatory zoning with a wavelength of about 3 μm (in olivine) should not have survived a diffusive exchange extending over 50 μm (the rim thickness).

The wavelength of oscillatory zoning in olivine does not differ strongly from that observed in augite (10 micrometers). As mentioned above, it can be scaled to D/V . Diffusivity in the melt is to the first order independent of the growing crystals, olivine and augite. The growth rates of olivine and augite are expected to be of the same order of magnitude since the crystals exhibit about the same size. We can calculate an olivine growth rate of about 7×10^{-8} m/s at 1080°C during its major growth stage.

4.2.3. Chemical gradients ahead of olivine: melt interface.

Chemical mapping of major and trace elements using the EDS equipment on the SEM, permits the observation of sharp chemical gradients at the rims of both olivine and augite, especially for P whose diffusivity in the melt is reputedly sluggish (Fig. 13). This feature indicates that growth rates were particularly rapid and diffusion could not erase such compositional excesses, neither during nor after growth. This feature is typically observed in experiments where quenching is possible but rarely under natural conditions. Subsolidus exchange in the melt (glass), if any, should have been much faster in the melt than in the crystals; subsolidus diffusion conflicts with this observation.

/Fig. 13: Chemical map Fe:Ti:P/

4.3 Mesostasis abundance

Mesostasis abundance relates to the packing efficiency or burial depth. Compared to other nakhlites, NWA 5790 is characterized by the high abundance of mesostasis, which is reflected in the overall chemical composition as well. The mesostasis of NWA 5790 is indistinguishable from that of MIL 03346 or NWA 817: the interspecimen variations are of the same magnitude as those recorded for one single sample and correspond to the analysis of a more or less crystallized fraction. The

composition of the whole rock indicates a large fraction of intercumulus liquid and the highest REE content. Mesostasis abundance, whole rock composition, thin olivine and augite rims, skeletal crystals and glassy proportion of the mesostasis indicate that NWA 5790 experienced the fastest cooling of any nakhlite. It thus supersedes MIL 03346 at the top of a nakhlite pile (Mikouchi et al, 2003).

4.4 Oxygen fugacity.

There are two classical ways of assessing the oxygen fugacity in SNCs. A first approach uses the composition of coexisting oxides (ilmenite and titanomagnetite). Szymanski et al. (2010) obtained oxygen fugacities in the range QFM to QFM-1 at a closure temperature of 710-810 °C for four different nakhlites. Unfortunately, the same calculation cannot be applied here for two reasons: i) the ilmenite exsolutions in titanomagnetite phenocrysts are too small to be analyzed accurately with EMP. ii) the titanomagnetite composition in the mesostasis differs from the phenocrysts and is highly variable, indicating that equilibrium did not prevail during this phase of crystallization.

Eu to Gd ratio and oxygen fugacity

A second way of assessing the oxygen fugacity is from the ratio of Eu to Gd in augite and coexisting melt, following McKay et al. (1994). Doing so, we assume that the mesostasis composition does not differ significantly in REE pattern from that of the melt from which augite crystallized. We obtain IW+3 (± 0.5) (or QFM -0.5) assuming a magmatic closure temperature (about 1050°C). All three nakhlites studied fall within 0.1 log unit, a very restricted range. These results compare quite well with those of Szymanski et al. (2010) who gives values of QFM -0.8 to +0.1 for four other

nakhlites using the Fe, Ti-oxide oxybarometer, despite the fact that the latter are for much lower temperatures (780 to 710 °C). However, if core augite is xenocrystic this procedure may not be legitimate.

Magnetic properties and oxygen fugacity

The magnetization of previously studied nakhlites is carried by titanomagnetite in variable amounts from about 0.3 to 1.5 wt. % (pure magnetite equivalent; Rochette et al. 2005). NWA 5790 shows intrinsic magnetic properties coherent with other nakhlites (Gattacceca et al., 2014) but with the highest magnetization of all nakhlites except MIL 03346 (which has a slightly higher saturation magnetization M_s but lower susceptibility, see Table 1). Among nakhlites, two groups, magnetite-rich and poor, correspond to MIL 03346-NWA 5790 and Governador-Lafayette-Nakhla, respectively, suggesting that the magnetite content, and thus oxygen fugacity, roughly increases up the magmatic pile. However, the deepest sample (NWA 998) appears also quite magnetite-rich, in an intermediate group with NWA 817 and Y-000593. Magnetite grain-size, as indicated by coercivity parameters, is homogeneous among nakhlites, two samples exhibiting significantly coarser grains: NWA 998 and Y-000593. Y-000593 is unlike other nakhlites, as a significant magnetic contribution arises from pyrrhotite (Funaki et al., 2002). M_s is potentially a more robust way than microscopy to estimate the amount of titanomagnetite present, as the grain size does not influence the estimate, while microscopy has a difficult time quantifying grains below 10 μm size. Magnetic domain state in NWA 5790 is pseudo-single domain with average magnetic grain size of the order of 1 μm (however, magnetic grain size may be smaller than real grain size if the grain exhibit ilmenite lamellae). On the other hand calculating the amount of titanomagnetite from M_s (instead of the pure magnetite equivalent mentioned above) necessitates the knowledge of average substitution. Assuming an average substitution of Uv63 in titanomagnetite based on

the few mesostasis analyses, leads to a titanomagnetite specific M_s of $45 \text{ Am}^2/\text{kg}$ (instead of 92 for pure magnetite). Therefore the measured M_s translates into 2.6 wt. % titanomagnetite, or 1.6 vol. %. This is slightly larger than the modal analysis estimate (0.3 vol. % as phenocrysts and 0.6 vol. % as fine grains in the mesostasis). This discrepancy is easily accounted for by the underestimated content of oxide in the mesostasis based on microscopic imaging. The higher content indicated by magnetism is coherent with the rather high content of TiO_2 in the bulk mesostasis analyses: 1.03 wt. % which corresponds to 5 % Ti-magnetite in the mesostasis or 2.4 % in the bulk rock (1.8 in the mesostasis plus 0.6 % as phenocrysts) in fairly good agreement with the estimate from magnetism.

4.5 Primary melt composition

According to their different phenocryst compositions, the eight different nakhlites may be derived from consanguineous parent melts differentiated to different extents. First of all, we must state clearly what parent melt means. If olivine and augite are not equilibrated they must have had two different parent melts, whose composition may be estimated.

Inferring nakhlite parental melts is difficult as these rocks are cumulates. For NWA 5790 we derived the parent melt compositions using a four step procedure: i) Add the adcumulus growth (augite and olivine rims) to the analyzed bulk mesostasis composition. ii) Add to this melt composition, the appropriate quantity of augite and olivine phenocrysts that precipitated in equilibrium with the melt. iii) Add more olivine and subtract some augite (core composition) to account for their partial resorption. iv) Add olivine until we obtain a melt composition in equilibrium with the most mafic olivine found in the other nakhlites ($\text{Mg}\# = 43$).

Step 1: To obtain the melt composition before rim crystallization of olivine and augite (adcumulus growth) we need to add the appropriate amounts of Fe-rich crystal rims. This requires the knowledge of i) the ratio of melt (mesostasis) to crystals (rims) and ii) the relative proportion of olivine and augite adcumulus growth. From the BSE images only, these ratios cannot be obtained accurately as the overgrowth rims of both olivine and augite are discontinuous and the conversion of surface to volume ratio is not straightforward in this particular case. The melt to crystal rim ratio is better constrained by equilibrium considerations (Mg#), the addition of olivine and augite (Mg# of 47 and 28 for augite and olivine respectively) yields an instantaneous melt in equilibrium with phenocryst rim. The augite to olivine ratio is constrained by the CaO content of the augite, which must reproduce the observations. We add olivine and augite in equilibrium with the melt incrementally to the mesostasis composition, and iterate step-by-step using a parameterized composition of both olivine and augite derived from the data of Toplis and Carroll (1995). The best fit is obtained for a mass fraction of crystals of 18 % with a mass ratio of augite to olivine of 91:9. This intermediate composition (J1) is listed in Table 10. At this stage we obtain Mg# of 28.3 and 47.0 for olivine and augite, respectively.

Step two consists of adding more augite and olivine to the melt until reaching an Mg# of 36 for olivine and 53 for augite in equilibrium with the melt. The difference with the last intercumulus growth stage is the augite to olivine ratio, which is expected to vary from about, 91:9 (as in the previous step) to 0:1, corresponding to the point when augite starts being resorbed. The best solution is obtained for another 7-wt. % crystallization, but the ratio of augite to olivine must be kept at 95:5 in order to keep an acceptable augite composition. We obtain Mg# of 53.6 and 36 for augite and olivine respectively. The composition of this equilibrium melt (J2) is listed in Table 10.

For steps three and four the scenario has to be changed to account for augite dissolution, which predates olivine crystallization rather than being coeval as suggested initially. After this event olivine and augite precipitated simultaneously with a constant mass fraction in the solid. The presence of olivine on the liquidus is probably due to decompression, while augite is saturated but with a composition different from that having been resorbed.

How much augite was dissolved is the only remaining question. The amount of augite is totally unconstrained except that the superheat necessary to dissolve augite is limited. More importantly, by subtracting augite (the dissolved fraction) it is impossible to generate melts that could be in equilibrium with the more mafic crystals observed in the other nakhlites or even with the core of augite xenocrysts found in NWA 5790. We must conclude that augite are true xenocrysts that crystallized previously from a less evolved melt.

To summarize, from the mesostasis composition we can calculate successive melts: before adcumulus crystallization (J1), before crystallization of olivine and augite (J2). For the sake of illustration we calculate the melt composition before the dissolution of 6 % core augite (J3) but as mentioned above this choice is not constrained. The compositions J1-J3 are reported in Table 10 and can be compared with previous estimates from the literature (Treiman, 1986-1993; Longhi and Pan 1989; Harvey and McSween 1992 b; Treiman et al. 1998; Treiman and Goodrich, 2001; Varela et al. 2001; Stockstill et al. 2005; Sautter et al. 2012).

The estimated parental melt obtained by this four-steps procedure, is drastically different from previous estimates for several reasons (Table 10). The major reason is that we constrained the parental melt to be in equilibrium with core olivine, whereas core augite is considered to be xenocrystic. Previous workers assumed that the parental melt was in equilibrium with core augite and considered that olivine

compositions (even the cores) resulted from secondary diffusional equilibration with the melt. In the case of NWA 5790, core augites are obviously xenocrystic and secondary diffusional equilibration of olivine can be rejected.

Therefore one obvious question arises: can we derive the melt composition in equilibrium with augite cores and can this melt after some evolution be parent to olivine phenocrysts? Depending on the extent of the melt evolution augite and olivine cores will be close to, or far from equilibrium with one another.

/Table 10: Parent melt composition/

Application of the model to other nakhlites:

For the other seven nakhlites, in agreement with compositions estimated by Treiman (1986) and investigated by Pan and Longhi (1989) the last magma batch had olivine on its liquidus and not augite, which favors the above scenario for the other nakhlites as well, whereas most authors assumed that augite was on the liquidus.

Unlike augite cores, olivine core compositions of the different nakhlites vary significantly (from Mg# 35 to 43) (Fig. 4) which suggests that they were derived from different magma batches, a possibility already suggested but usually refuted because of the too tenuous evidence (Treiman, 2005). It is possible that some of the variability between the different nakhlites relates to variable amounts of resorbed augite. It follows that the composition we derived (J2) can be valid for the last magma batch from which NWA 5790 crystallized after the last (minor) resorption of augite. Our parent melt estimates differ significantly from estimates for the other nakhlites as we consider here olivine as phenocrystic and augite as xenocrystic. Still the question of

the melt parent to augite cores remains. The augite core compositions in the different naxhlites vary slightly from Mg# = 62.5 to 62.9 in Nakhla, Governador Valadares, Lafayette, Y-000593 and MIL 03346, to significantly different values of 64.5 in NWA 998, and 66.5 in NWA 817 on one hand and 60 in NWA 5790 on the other. Therefore the melts parent to the augite cores are certainly less variable than the melts parent to olivine, which are fractionated to variable extents.

The melt parent to augite cores can be calculated using the same procedure as above. Starting from J2 we incrementally add augite and olivine. Doing so we make a systematic error as we neglect augite resorption (out of equilibrium) and replace this process by less augite crystallization (at equilibrium). We obtain the composition J4 (Table 10) that is in equilibrium with the most mafic pyroxenes cores of NWA 817. The less mafic augite cores would correspond to intermediate melt compositions. Not surprisingly this composition falls within the range of the other parent melts, however the amount of CaO and FeO are low and Al₂O₃ is too high. The degree of crystallization necessary to obtain this composition starting from J2, is 22 % augite and no olivine, a moderate amount. The trace element composition of this melt will not be strongly different from the mesostasis as illustrated by the K₂O content which is decreased from 1.6 % in the mesostasis to 1.04 % in J4. This K₂O content is intermediate between that obtained by Treiman and Goodrich (2001) and other workers (Table 10). The former value was derived from the composition of melt inclusions in olivine while the latter was derived mostly from pyroxene compositions. It is worth pointing out that the absence of a Eu anomaly in the mesostasis proves that plagioclase was not significantly fractionated. The naxhlite parent melts J4 has a normative composition of 42 % feldspar, 41 % pyroxene and 14 % olivine and an Mg# of 30.5. This cannot be the product of melting of a normal mantle (i.e. a mixture

of dominant olivine, pyroxene and minor plagioclase). At a low melting fraction, the melt will be devoid of normative olivine whereas at very high melting fractions (necessary for a high olivine content) the feldspar fraction should be very low. This particular melt composition results from a strong FeO enrichment in the source, which makes olivine far more fusible than in more MgO rich sources; alternatively the parent melt (J4) is already fractionated to a significant extent. These inferences are based on the primitive Martian mantle estimates (Longhi et al. 1992; Sanloup et al. 1999; Ghosal et al. 1998) with an Mg# of 72-80 indicating that the melt was not a primitive mantle product (e.g. Treiman 2005).

4.6 NWA 5790 petrogenesis

The petrogenesis of nakhlites has been the concern of a number of previous works (see Treiman, 2005 and references therein). Since we consider that augite cores are xenocrystic, previous petrogenetic scenarios must be modified.

In a first stage augite crystals (Mg# of 60) grew alone from a relatively evolved, Fe-rich mafic melt at depth, forming augite glomerocrysts in a cumulate layer at the bottom of a magma chamber, as indicated by their close association in clusters (notice that in a mature cumulate we should not be able to distinguish clusters) (Treiman 1990; Sautter et al 2002, 2006). A subsequent magma batch disrupted this crystal conglomerate during a violent event, breaking some of the augite crystals of Mg# 60. Augite being out of equilibrium with this new batch dissolved steadily developing scalloped resorbed boundaries in addition to evidence of breakage. The partial dissolution of the augite cumulate and significant decompression brought olivine onto the liquidus and supercooled the melt significantly. Olivine (Mg# 35)

precipitated. After partial augite resorption, a short episode of new augite crystallization occurred and crystals settled as soon as their size was large enough. It seems that olivine and augite resumed growth simultaneously or nearly so. Finally the crystals trapped in a new cumulate, finished their growth in a closed system forming thin rims around both augite and olivine. The cumulate cooled rapidly hindering compaction and permitting the preservation of a large fraction of mesostasis. The succession of augite crystallization alone and olivine plus augite crystallization can be understood if the two stages proceeded under different pressures. If the pressure exceeds that for the existence of a peritectic, then augite alone will precipitate. At lower pressure, the eutectic is displaced and olivine is on the liquidus, followed by augite.

The following scenario of nakhlite magma evolution has been extensively discussed previously. Because the texture and composition of NWA 5790 is quite similar, the reader is referred to the work of Day et al. (2006) for a complete discussion and additional details. The succession of events is as follows:

- a- partial melting, melt extraction and ascent of nakhlite parental magma from a LREE depleted mantle source (e.g. Shih et al. 1999).
- b- crystallization of cumulus augite Mg #66-60 at some depth in a magma chamber. According to the different compositions of augite cores in the eight nakhlites several batches of melts and compositional evolution are expected.
- c- A final magma-mixing event produced the entrainment of cumulus crystals (augite) within the melt towards the surface. Decompression and partial augite dissolution brought olivine to the liquidus in a strongly supercooled melt. Augite growth resumed concomitantly.
- d- Extrusion and surface emplacement as thick lava flows, crystal settling, compaction and decreasing degree of equilibration from bottom to top throughout the

nakhlite flow. A number of successive flows may account for the small differences between the different nakhlites (Mg# of augite and olivine) corresponding to successive flows in a lava pile. Successive flows also explain the lack of correlation between olivine composition and mesostasis abundance.

NWA 5790 possibly represents a quenched margin with the fastest cooling rate. Since NWA 5790 is a cumulate, the magma parent to accumulation must have flowed away otherwise it would never have cooled fast enough in order to trap a significant fraction of vitrophyric mesostasis.

-e- Secondary hydrothermal alteration after cooling of the flow.

-f- Impact release of the nakhlites from Mars 10-11 Ma ago.

The study of NWA 5790 sheds new light on stages b-d, providing evidence of a new magma batch with more evolved liquid composition compared to the nakhlite parent magma but still less evolved than intercumulus liquid that produced hedenbergitic overgrowth. Finally there is no trace of iddingsite formation, possibly replaced by discreet amphibole formation in association with smectite (?) in fractures. This observation suggests that NWA 5790 may have been buried at a greater depth when hydrothermal alteration occurred (higher temperature), and is best explained by NWA 5790 belonging to the top-most position in the bottom-most flow (Figure 14).

5. CONCLUSIONS

There is no doubt that NWA 5790 is a new nakhlite unpaired with any other previously studied nakhlites. It likely comes from the same magmatic complex on Mars, which has been ejected by one single impact event. It supersedes MIL 03346 as the least reequilibrated, the least compacted, and the fastest cooled nakhlite. It shows the lowest degree of preferred orientation of any nakhlite and shares with MIL 03346 the highest Ti-magnetite amount and thus oxygen fugacity. It provides evidence for complex magma mixing prior to eruption to the surface recorded in augite cores with a residence time in the magma chamber short enough to prevent Fe-Mg homogenization. Olivine is not truly co-magmatic with augite since the latter exhibited two stages of growth separated by some resorption. A similar scenario may be true for some other nakhlites at least, where the olivine status has been discussed, especially those with a significant mesostasis fraction.

According to the texture and the chemical composition of phases in NWA 5790, augite appears to be xenocrystic while olivine is indigenous. It may be more accurate to say that the nakhlite magmas result from two stages of magmatic evolution: one at high pressure, parent to the mafic cores of augites, the other one at a much lower pressure parent to olivine and a second growth stage of augite. When compared to other nakhlites it appears that augite (Mg# from 66 to 60) and olivine (Mg# from 43 to 34) differ among the different rocks and are in disequilibrium with one another to various extents. The olivine compositions indicate that the second stage parent magmas are differentiated to various extents. Melts parent to augite are less fractionated. The magma parent to NWA 5790, the most evolved nakhlite, can be derived from a more primitive melt, parent to the most primitive augites (in the other nakhlites) by fractional crystallization of augite (on the order of 30 %). The more

fractionated character of NWA 5790 compared to NWA 817 (for instance) can be accounted for by the fractionation of a significant amount of augite.

The significant geochemical differences and their obvious consanguinity suggest that the different nakhlites correspond to periodic discharges from a magma chamber at depth where augite crystallized. After disrupting augite cumulates, the magma is expelled and olivine crystallizes during this last episode. Final accumulation of augite and olivine permits trapping of variable amounts of mesostasis depending on the extent of compaction (Fig. 14). Within one flow the position can be estimated from the mesostasis abundance. Therefore, NWA 5790 is probably from the topmost of one such flow according to its large mesostasis fraction. The absence of low temperature pervasive alteration (smectite/iddingsite) and the presence instead of a mixture of amphibole with hydrous phases suggests that it belongs to the deepest flow in the stack sampled so far. This scenario is summarized in figure 14: The different nakhlites are grouped in one top flow comprising MIL 03346, Y-000593 Governador Valadares, Lafayette and Nakhla with one single augite core composition and abundant smectite, an intermediate flow with NWA 817 and NWA 998 and a lower flow with NWA 5790.

/ Fig. 14 The nakhlite pile revisited/

Acknowledgements: A. Habibi is greatly acknowledged for donating the reference specimen of NWA 5790. We are indebted to Kevin Righter and the meteorite curation group for the loan of a polished section of MIL 03346. US Antarctic meteorite samples are recovered by the Antarctic Search for Meteorites (ANSMET) program, which has been funded by NSF and NASA, and characterized and curated by the Department of Mineral Sciences of the Smithsonian Institution and Astromaterials Curation Office at NASA Johnson Space Center. ENS Lyon is acknowledged for the loan of a polished section of NWA 817. J-P. Lorand provided a reference calibration sample for olivine. R. Hewins corrected carefully our frenglish and made helpful

suggestions. M. Fialin and N. Rividi are thanked for assistance on the microprobe. We thank C. Herd for the editorial handling and careful editing, J. Hammer and two anonymous reviewers for constructive comments. We gratefully acknowledge the Programme National de Planétologie (CNRS-INSU) for financial support.

ACCEPTED MANUSCRIPT

References

- Allègre C.J., Provost A. and Jaupart C. (1981) Oscillatory zoning : a pathological case of crystal growth. *Nature* **294**, 223-228.
- Anand M., Williams C.T., Russell S.S., Jones G., James S., and Grady M.M. (2005) Petrology and Geochemistry of Nakhilite MIL 03346: A New Martian Meteorite From Antarctica. *Lunar and Planetary Science Conference* **36**. Lunar Planet. Inst., Houston. #1639(abstr.).
- Baghdadi B., Jambon A., Barrat J-A. (2015) Metamorphic angrite Northwest Africa 3164/5167 compared to magmatic angrites. *Geochim. Cosmochim. Acta*, **168**, 1-21.
- Barrat J.A., Jambon A., Bohn M., Blichert-Toft J., Sautter V., Göpel C., Gillet Ph., Boudouma O., and Keller F. (2003) Petrology and geochemistry of the unbrecciated achondrite North West Africa 1240 NWA 1240: an HED parent body impact melt. *Geochim. Cosmochim. Acta*, **67**, 3959-3970.
- Barrat J. A., Yamaguchi A., Greenwood R. C., Bollinger C., Bohn M. and Franchi I. A. (2009) Trace element geochemistry of K rich impact spherules from howardites. *Geochim. Cosmochim. Acta*, **73**, 5944–5958.
- Barrat J.A., Zanda B., Moynier F., Bollinger C., Liorzou C., and Bayon G. (2012) Geochemistry of CI chondrites: Major and trace elements, and Cu and Zn isotopes. *Geochim. Cosmochim. Acta*, **83**, 79-92.
- Berkley, J.L., Keil, K., Prinz, M. (1980). Comparative petrology and origin of Governador Valadares and other nakhlites. *Lunar Planet. Sci.* **XI**. Lunar Planet. Inst., Houston, 1089–1102.
- Bertka, C.M., Fei, Y., (1997). Mineralogy of the martian interior up to core–mantle boundary pressures. *J. Geophys. Res.* **102**, 5251–5264.
- Collinson, D.W. (1997). Magnetic properties of Martian meteorites: implications for an ancient Martian magnetic field. *Meteorit. Planet. Sci.* **32**, 803-811.
- Cotten J., Ledez A., Bau M., Caroff M., Maury R. C., Dulski P., Fourcade S., Bohn M., and Brousse R. (1995). Origin of anomalous Rare-Earth Element and Yttrium Enrichments in Subaerially Exposed Basalts - Evidence from French-Polynesia. *Chem. Geol.* **119**, 115-138.
- Day J.M.D., Taylor L.A., Floss C., and McSween H. Y Jr. (2006) Petrology and chemistry of MIL 03346 and its significance in understanding the petrogenesis of nakhlites on Mars. *Meteorit. Planet. Sci.* **41**, 581-606.
- Dreibus G. and Wänke H. (1982) Parent body of the SNC meteorites: Chemistry, Size and Formation. *Meteoritics* **17**, 207-208.
- Friedman-Lentz, R.C., Taylor, G.J., Treiman, A.H., (1999). Formation of a martian pyroxenite: a comparative study of the nakhlite meteorites and Theo's Flow. *Meteorit. Planet. Sci.* **34**, 919–932

- Funaki M., Hoffmann V. and Imae N. (2009). Estimate of the magnetic field of Mars based on the magnetic characteristics of the Yamato 000593 Nakhlite. *Meteorit. Planet. Sci.* **44**: 1179-1191.
- Gattacceca J., Rochette P., Denise M., Consolmagno G., Folco L. (2005) An impact origin for the foliation of chondrites. *Earth Planet. Sci. Lett.* **234**, 351– 368
- Gattacceca J., Rochette P., Gounelle M., van Ginneken M. (2008) Magnetic anisotropy of HED and Martian meteorites and implications for the crust of Vesta and Mars, *Earth Planet. Sci. Lett.* **270**, 280-289.
- Gattacceca, J., P. Rochette, R. B. Scorzelli, P. Munayco, C. Agee, Y. Quesnel, C. Cournède, and J. Geissman 2014, Martian meteorites and Martian magnetic anomalies: A new perspective from NWA 7034, *Geophys. Res. Lett.*, **41**, doi:10.1002/2014GL060464
- Ghosal, S., Sack, R.O., Ghiorso, M.S., Lipschutz, M.E., 1998. Evidence for a reduced, Fe-depleted martian mantle source region of shergottites. *Contrib. Miner. Petrol.* **130**, 346–357.
- Gillet P., Barrat J-A., Deloule E., Wadhwa M., A. Jambon A. , Sautter V. , Devouard B., Neuville D., Benzerara K., Lesourd M. (2002). Aqueous alteration in the Northwest Africa 817 (NWA 817) Martian Meteorite. *Earth Planet. Sci. Lett.* **203**: 431-444.
- Goodrich C.A., Treiman A.H., Filiberto J., Gross J. , and Jercinovic M.(2013) K₂O-rich trapped melt in olivine in the Nakhla meteorite: Implications for petrogenesis of nakhrites and evolution of the Martian mantle. *Meteoritics Planet. Sci.* **48**, 2371-2405.
- Greenwood J.P., Mojzsis S.J., Coath C.D. (2000). Sulfur Isotopic Compositions of individual Sulfides in Martian Meteorites ALH84001 and Nakhla: Implications for Crust-regolith exchange on Mars. *Earth Planet. Sci. Lett.* **184**: 23-35.
- Greshake A., Stephan T. and Rost D.(2000) Combined TEM and TOF-SIMS study of symplectite exsolutions in olivine from the Martian meteorites Nakhla and Governador Valadarez. *Lunar and Planetary Science Conference* **31**. Lunar Planet. Inst., Houston. #1150 (abstr.).
- Hammer J.E. and Rutherford M.J. (2005) Experimental crystallization of fe-rich basalt: Application to cooling rate and oxygen fugacity of Nakhlite MIL03346 *Lunar Planet. Sci.* **XXXVI**. Lunar Planet. Inst., Houston. #1999(abstr.).
- Harvey R. P. and McSween H. Y. (1992)a. Petrogenesis of the nakhlite meteorites: Evidence from cumulate mineral zoning. *Geochim. Cosmochim. Acta* **56**: 1655–1663.
- Harvey R. P. and McSween H. Y. (1992)b. The parent magma of the nakhlite meteorites: Clues from melt inclusions. *Earth Planet. Sci. Lett.* **111**: 467–482.
- Huber L., Irving A.J., Maden C. and Wieler (2012) R. Noble Gas Cosmic Ray Exposure Ages of four unusual Martian Meteorites: Shergottites NWA 4797, NWA 5990, NWA 6342 and Nakhlite NWA 5790. *Lunar and Planetary Science Conference* **43** (Abstr.) 1408.
- Imae N. and Ikeda Y. (2007). Petrology of the Miller Range 03346

- nakhlite in comparison with the Yamato 000593 nakhlite. *Meteorit. Planet. Sci.* **42**: 171–184.
- Jambon A., Barrat J-A, O. Boudouma O., Fonteilles M., Badia D., Göpel C. and Bohn M. (2005). Mineralogy and Petrology of the Angrite North West Africa 1296. *Meteorit. Planet. Sci.* **40**: 361-375.
- Jelinek V. (1981) Characterization of the magnetic fabric of rocks. *Tectonophysics* **79**, 63-67.
- Longhi, J., Pan, V., (1989). The parent magmas of the SNC meteorites. *Lunar Planet. Sci.* **XIX**. Lunar Planet. Inst., Houston. 451–464.
- Longhi, J., Knittle, E., Holloway, J.R., Wänke, H., (1992). The bulk composition, mineralogy, and internal structure of Mars. In: Kiefer, H.H., Jakosky, B.M., Snyder, C.W., Matthews, M.S. (Eds.), Mars. University of Arizona Press, pp. 184–208.
- McKay G., Le L., Wagstaff J. and Crozaz G. (1994) Experimental partitioning of rare earth elements and strontium: Constraints on petrogenesis and redox conditions during crystallization of Antarctic angrite Lewis Cliff 86010. *Geochim. Cosmochim. Acta*, **58**. 2911-2919.
- McKay G., Mikouchi T., and Schwandt C. (2006) Additional Complexities in Nakhrites Pyroxenes : a Progress (?) Report. *Lunar and Planetary Science* **37**, #2435
- McSween, H.Y. Jr, (1994). What We Have Learned About Mars From SNC Meteorites. *Meteoritics* **29**, 757-779.
- Mikouchi, T., Yamada, I., Miyamoto, M., (2000). Symplectic exsolution in olivine from the Nakhla martian meteorite. *Meteorit. Planet. Sci.* **35**, 937–942.)
- Mikouchi T., Koizumi E., Monkawa A., Ueda Y., and Miyamoto M. (2003). Mineralogical Comparison of Y-000593 With Other Nakhrites: Implications for Relative Burial Depths of Nakhrites *Lunar and Planetary Science Conference* **35**. Lunar Planet. Inst., Houston. # (abstr.).
- Mikouchi T., Miyamoto M., Koizumi E., Makishima J. and McKay G. (2006) Relative Burial Depths of Nakhrites: An Update. *Lunar and Planetary Science Conference* **37**. Lunar Planet. Inst., Houston. (abstr.)#1865.
- Mikouchi T., Sugiyama K., Kato Y., Yamaguchi A., Kaneda K. (2009) Calcium Silico-Phosphate in Angrite revisited. *72nd Annual Meteoritical Society Meeting*. Abstract 5351.
- Nakamura N., Unruh D.M., Tatsumoto M. and Hutchison R. (1982). Origin and Evolution of the Nakhla Meteorite inferred From the Sm-Nd and U-Pb Systematics and REE, Ba, Sr, Rb and K Abundances. *Geochim. Cosmochim. Acta* **46** : 1555-1573.
- Nyquist L. E., Bogard D. D., Shih C-Y., Greshake A., Stoffler D., and Eugster O. (2001). Ages and geologic histories of Martian meteorites. In *Chronology & Evolution of Mars (ISSI)* **96**:105–164.
- Rochette P., Gattacceca J., Chevrier V. and Lorand J.P. (2005). Matching Martian crustal magnetization and meteorite magnetic properties, *Meteorit. Planet. Sci.*, **40**: 529-540.
- Sanloup C., Jambon A., Gillet P. (1999) A simple chondritic model of Mars. *Phys. Earth Planet. Int.* **112** , 43–54.

- Sautter V., Barrat J-A., Jambon A., M. Javoy M., Lorand J-P., Gillet P., Joron J-L. & Lesourd M. (2002). A new Martian meteorite from Morocco: the nakhlite North West Africa 817. *Earth Planet. Sci. Lett.* **195** : 223-238.
- Sautter V., Jambon A., and Boudouma O. (2006). Cl-amphibole in the Nakhlite MIL 03346: Evidence for Sediment Contamination in a Martian Meteorite. *Earth Planet. Sci. Lett.* **252**: 45–55.
- Sautter V., Toplis M.J., Lorand J-P., and Macri M. (2012). Melt inclusions in augite from the nakhlite meteorites: A reassessment of nakhlite parental melt and implications for petrogenesis. *Meteoritics & Planetary Science* **47**, 330–344
- Shih C.-Y., Nyquist L.E. and Wiesmann H. (1999). Samarium-Neodymium and Rubidium-Strontium Systematics of Nakhlite Governador Valadares. *Meteorit. Planet. Sci.* **34** : 647-655.
- Shih C.-Y., Wiesmann, H., Nyquist, L.E., Misawa, K., (2002). Crystallization age of Antarctic nakhlite Y-000593: further evidence of nakhlite launch pairing. *NIPR Symposium on Antarctic Meteorites XXVII*, 151–153.
- Shih, C.-Y., Nyquist, L. E. & Reese, Y. (2006). Rb-Sr and Sm-Nd Isotopic Studies of Antarctic Nakhlite MIL 03346. *LPSC 37*, (Abst.) #1701.
- Shih, C.-Y., Nyquist, L. E. & Reese, Y. and Jambon A. (2010). Sm-Nd Isotopic Studies of two Nakhrites, NWA 5790 and NAKHLA. *LPSC 41*, (Abst.) #1367.
- Stockstill K. R., McSween H. Y., and Bodnar R. J. (2005). Melt inclusions in augite of the Nakhla Martian meteorite: Evidence for basaltic parental melt. *Meteorit. Planet. Sci.* **40**, 377–396.
- Szymanski A., Brenker F.E., Palme H. and El Goresy A. (2010) High oxidation state during formation of Martian nakhrites. *Meteorit. Planet. Sci.* **45**, 21–31.
- Tarling, D.H., Hrouda, F., (1993). The magnetic anisotropy of rocks. Chapman & Hall, London. 217 p
- Tomkinson T., Lee M.R., Mark D.F., Dobson K.J., Franchi I.A. (2015). The Northwest Africa (NWA) 5790 meteorite: A mesostasis-rich nakhlite with little or no Martian aqueous alteration. *Meteorit. Planet. Sci.* **50**, 287–304. doi: 10.1111/maps.12424
- Toplis M. J. and Carroll M. R. (1995). An Experimental Study of the Influence of Oxygen Fugacity on Fe-Ti Oxide Stability, Phase Relations and Mineral-Melt equilibria in Ferro-Basaltic Systems. *J. Petrol.* **36**:1137–1170.
- Treiman A. H. (1986). The Parental Magma of the Nakhla Achondrite: Ultrabasic Volcanism on the Shergottite Parent Body. *Geochim. Cosmochim. Acta* **50**: 1061–1070.
- Treiman A. H. (1990). Complex petrogenesis of the Nakhla (SNC) meteorite: Evidence from Petrography and Mineral Chemistry. *Lunar Planet. Sci.* **XX**. Lunar Planet. Inst., Houston. pp. 273–280.
- Treiman A. H. (1993). The parent magma of the Nakhla SNC meteorite, inferred from magmatic inclusions. *Geochim.*

- Cosmochim. Acta*, **57**: 4753–4767.
- Treiman A.H. (2005). The Nakhlite Meteorites: Augite-rich igneous rocks from Mars. *Chem. Erde*, **65**: 203-270.
- Treiman A. H. and Goodrich C. (2001). A parent magma for the Nakhla Martian meteorite: Reconciliation of estimates from 1-Bar experiments, magmatic inclusions in olivine, and magmatic inclusions in augite (abstract #1107). 32nd Lunar and Planetary Science Conference.
- Wadhwa M. and Borg L. E.,(2006) Trace Element and $\epsilon^{142}\text{Nd}$ Systematics in the Nakhlite MIL 03346 and the Orthopyroxenite ALH 84001: Implications for the Martian Mantle. *Lunar and Planetary Science Conference* **37**, #2045.
- Zhang Y (1993) A Modified Effective Binary Diffusion Model. *J. Geophys. Res.* **98**, 11901-11920.

ACCEPTED MANUSCRIPT

FIGURE CAPTIONS.

Figure 1: a) BSE image of section A. Notice the dominant euhedral augites (light grey), a few subhedral olivines (Ol) and large mesostasis pools with numerous dendritic crystals. Tm = titanomagnetite. B) False color image of section B (Red = Ca, Green = Fe, Blue = Si. Notice the rounded augites included in olivines (end of white lines).

Figure 2: BSE image, detail of figure 1a, top right, contrast enhanced. Note the irregular zoning of augite and its iron enriched rim (white fringe). The mesostasis contains chains of olivine and ferro augite as well as a few oxides.

Figure 3: Zoning profiles in both olivine and augite. Olivine cores exhibit a constant composition with an iron-enriched rim of about 50 micrometers, much thinner than in olivines of other mesostasis-bearing nakhlites. Augite cores are more complex, revealing successive growth stages (separated by the dashed lines). Note the slight Mg depression in the center of core 1 as already noted in some other nakhlites (see Treiman, 2005). Core 2 (Mg# 54) corresponds to some overgrowth on the more magnesium rich core 1 (Mg# 58-60). The augite rim is only 30 micrometers wide and corresponds to closed system final growth.

Figure 4: Augite compositions compared to MIL 03346 augites (core, rim and mesostasis; Day et al. 2006). Mesostasis crystals are generally too small to be analyzed by EMP.

Figure 5: Oscillatory zoning of both augite (a) and olivine (b). Notice the different scales and the different wavelengths of oscillations. a) Augite, same profile as figure 3. Concentrations for Si, Al, Fe and Ca, as measured without corrections. b) Olivine. The Mg variations are corrected for long-range zoning and short-range noise (see on-line supplement). The presence of fine scale compositional oscillations in olivine indicates that rim zoning cannot result from subsolidus diffusional exchange. MgO range in olivine core 14.7 ± 0.2 wt. %.

Figure 6: BSE images of mesostasis shows chains of silicates (ferroaugite and fayalite), skeletal Ti-magnetite and poorly crystallized feldspathic background (black). The inset (top left) with higher brightness shows zoned feldspar in the mesostasis and interstitial silica-feldspathic glass (scale bar is 20 micrometers).

Figure 7: BSE image of alteration (white) filling cracks in olivine and at the boundary between olivine and augite. The polyphase character of alteration product is visible in the inset.

Figure 8: Trace element patterns in NWA 5790. **A**: Chondrite normalized REE pattern of the bulk of NWA 5790 compared to other nakhlites. The REE element abundances are the highest among nakhlites as expected from the high mesostasis fraction. Notice the similarity of the pattern with NWA 817,

Sautter et al. (2002). Data for Nakhla from Dreibus et al. (1982). **B**: Spider diagram normalized to Nakhla. The concentration of incompatible elements is controlled by the abundance of mesostasis. Note that the most incompatible elements exhibit a stronger enrichment in NWA 5790 indicating that the mesostasis of NWA 5790 is more differentiated than that of either NWA 817 or MIL 03346. Data for NWA 817 after Sautter et al. (2002)

Figure 9: Sr vs Al_2O_3 abundance in nakhlites compared to shergottites, showing the different Sr/ Al_2O_3 ratios, which are significantly fractionated for nakhlites.

Figure 10: Chondrite normalized REE pattern of separate phases, as obtained by LA-ICP-MS. The bulk rock pattern (Fig. 8A) is clearly dominated by the mesostasis contribution. Note the absence of Eu anomaly in the mesostasis. The light REE in olivine of NWA 817 and MIL 03346 are affected by the presence of alteration (see text).

Figure 11: The equilibrium between olivine and augite according to Toplis and Carroll (1995) corresponds to the thick plain line. It appears clearly that olivine and augite core compositions of some of the nakhlites are not in equilibrium (black squares; e.g. Lafayette). The red full circles correspond to adjacent crystals measured in NWA 817 by Sautter et al. (2002) and illustrate intercumulus closed system crystallization. Minor deviation from the equilibrium line may result from oscillatory zoning. Open circles/squares

for NWA 5790 pairs of olivine/augite crystals (intimate contact) illustrate a similar trend. 998 = NWA 998, Y = Y-000593; MIL = MIL 03346; 817 = NWA 817; GV = Governador Valadares.

Figure 12: Equilibration temperature vs. Mg# of melt, olivine and augite, derived from the experimental data of Toplis and Carroll (1995) (plain lines: best fit; fields: data dispersion). Outlined points are for contacting crystals in NWA 5790. The augite cores correspond to high temperatures of more magnesian melts, not in equilibrium with olivines derived from less mafic melts at a lower temperature. Crystals in the mesostasis appear to be in equilibrium. Data points from zoned rims in NWA 5790 suggest that overgrowths of olivine and augite may be in equilibrium. The dashed line separates cores from final overgrowth.

Figure 13: False color chemical map of Fe:Ti: P (pink :orange and blue); showing olivine (pink) augite (crimson) and Ti-magnetite (orange). The P rimming (blue) of both olivine and augite appears clearly. Detail from figure 1b, at left. Scale bar is one hundred micrometers. The preservation of chemical profiles in glass rimming crystals is unusual, as it requires very rapid cooling.

Figure 14: The nakhlite pile revisited. The different compositions of augite and olivine cores suggest that there are at least three distinct lavas flows. The textural and compositional kinship supports one common pile. NWA 5790 despite of its top-of-pile characteristics is placed at the bottom

because of the absence of pervasive low temperature alteration. It is interpreted as the top of the deepest flow sampled so far. Modified after Mikouchi et al. (2003).

ACCEPTED MANUSCRIPT

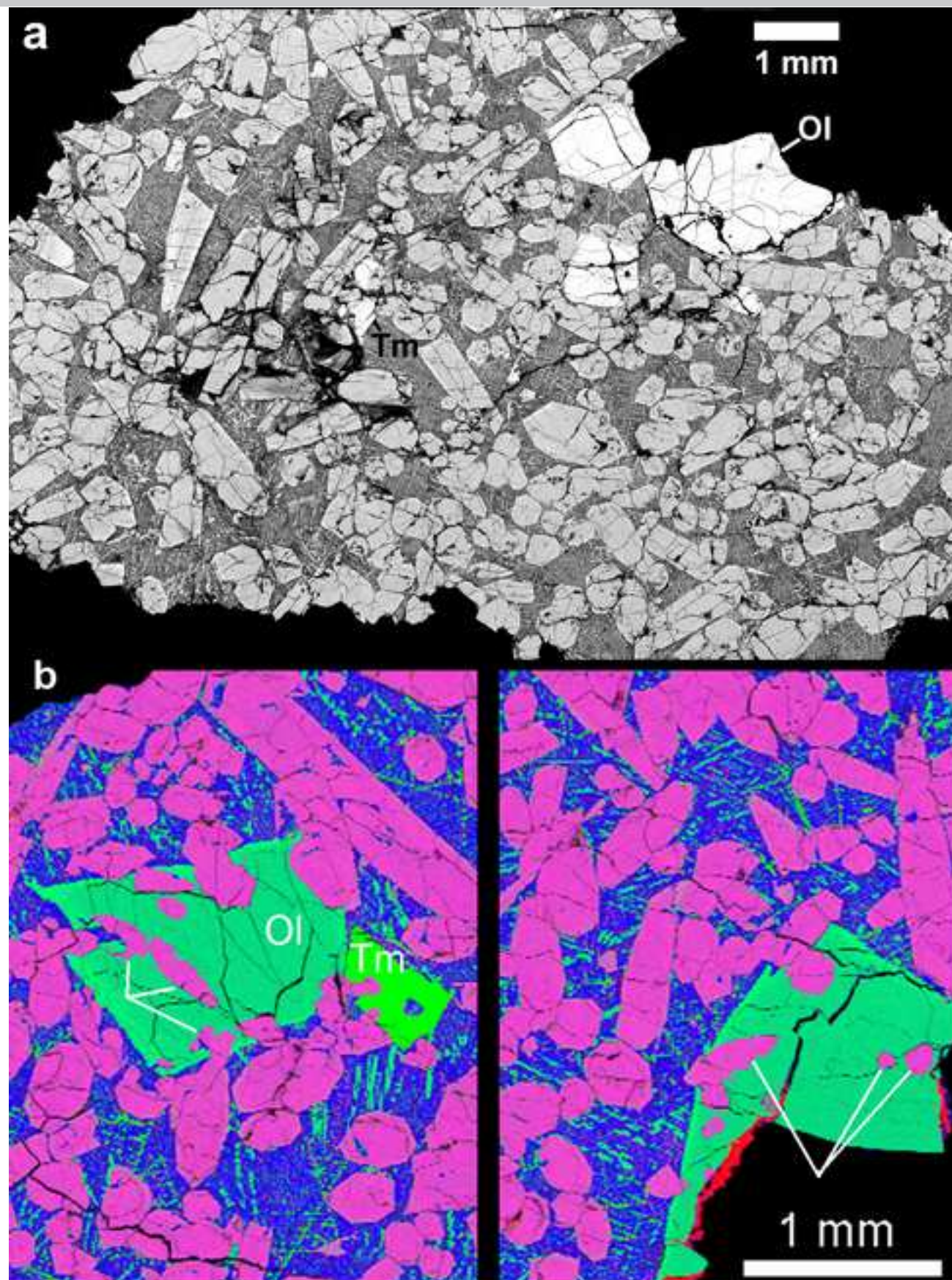
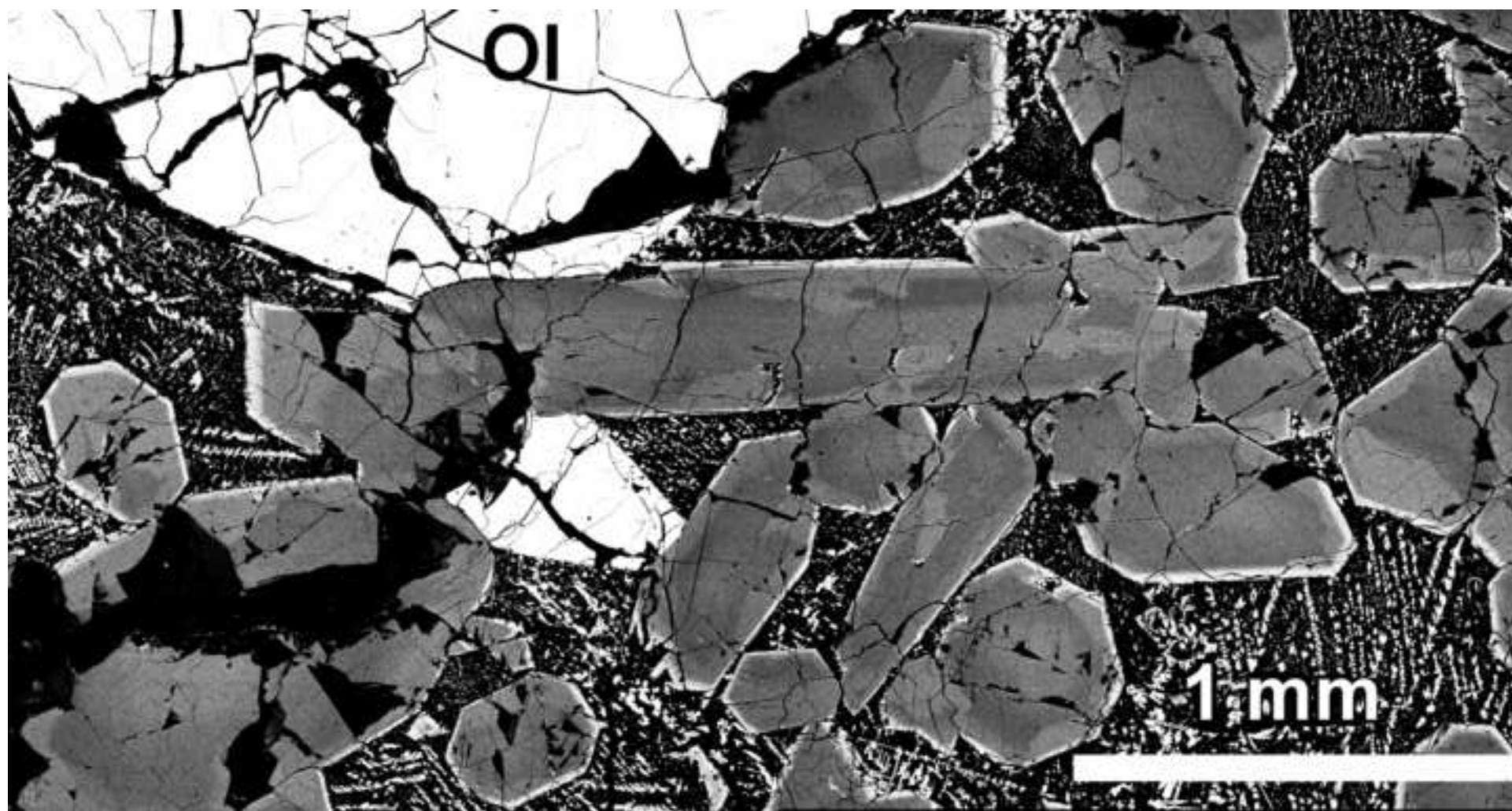


Figure 1 . Jambon et al.



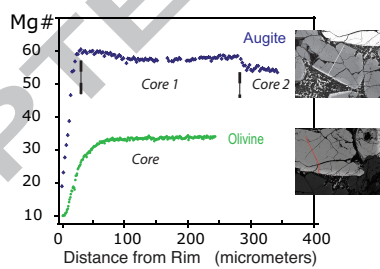
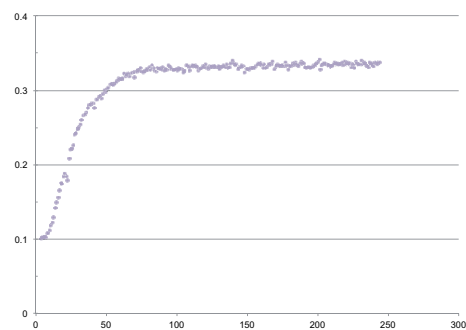


Figure 3. Jambon et al.



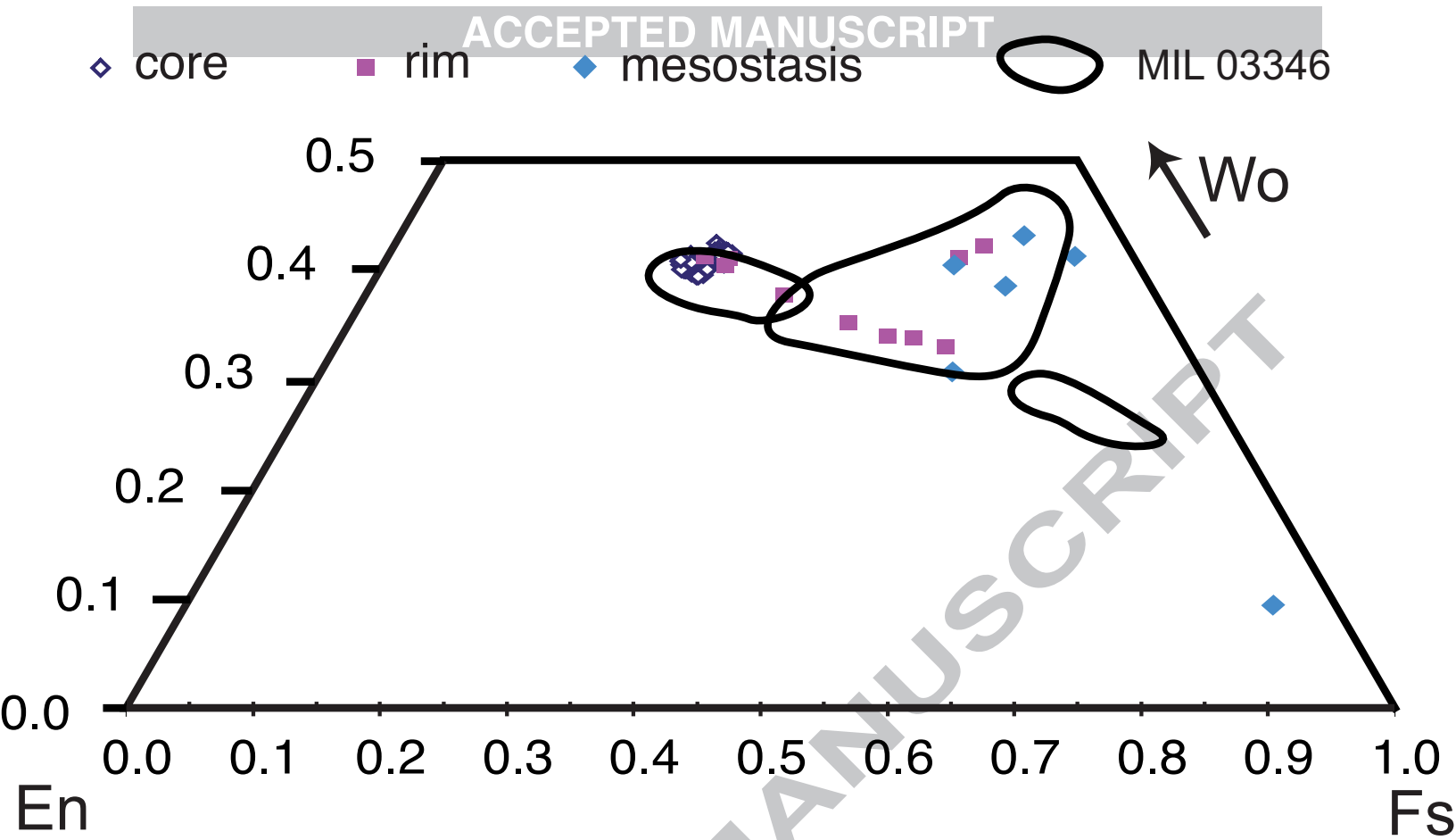


Figure 4. Jambon et al.

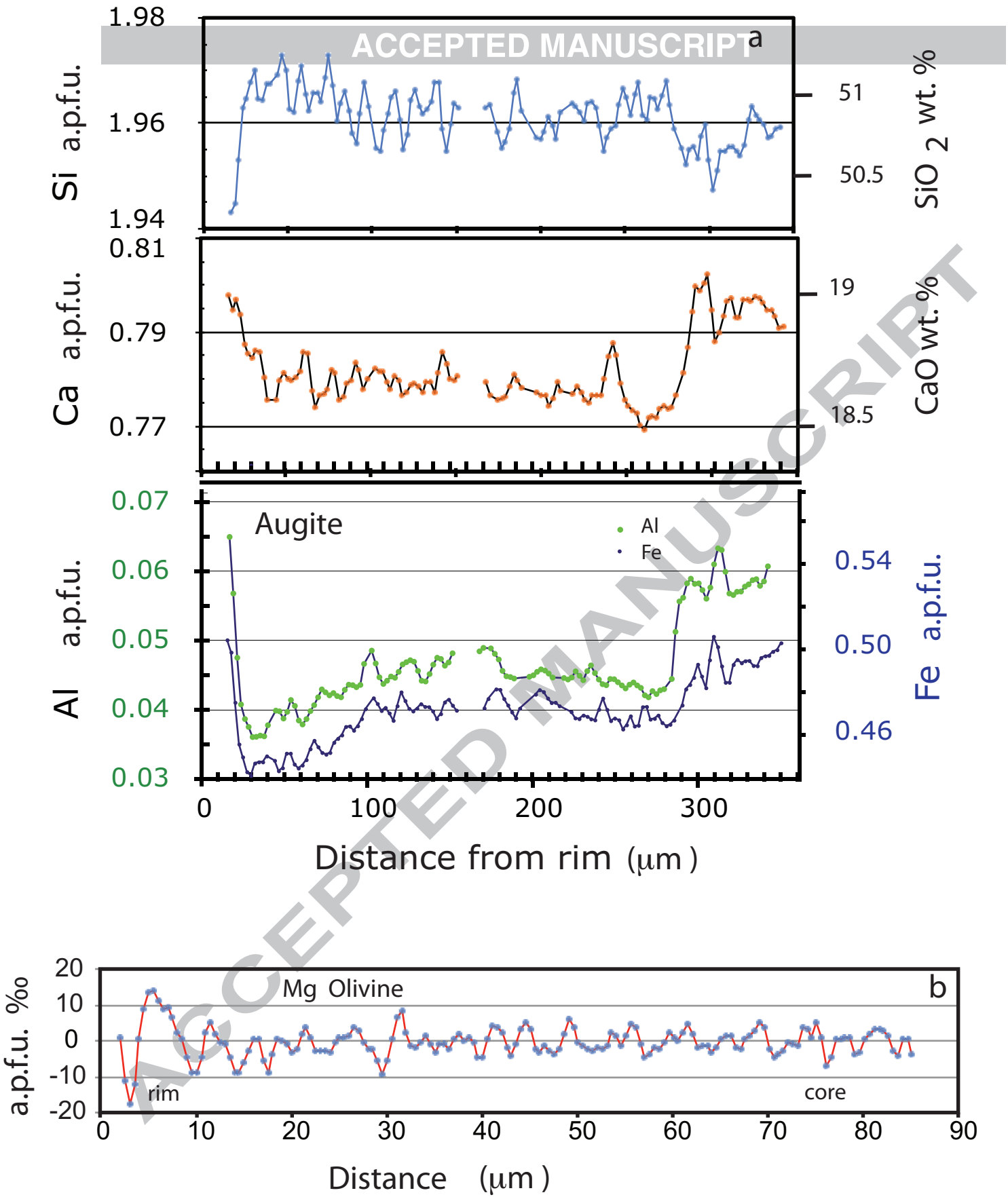


Fig. 5 : jambon et al.

Figure 6

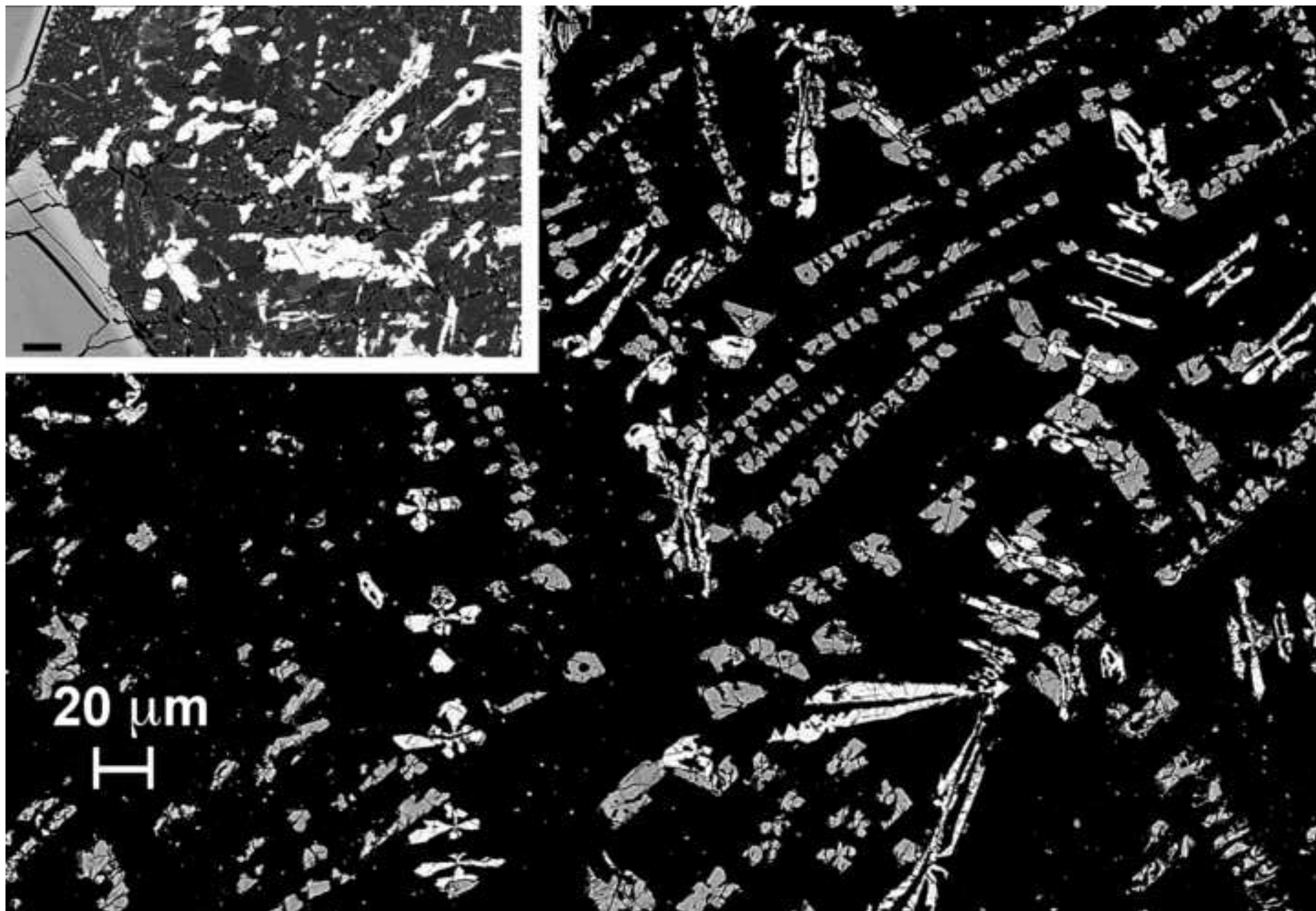
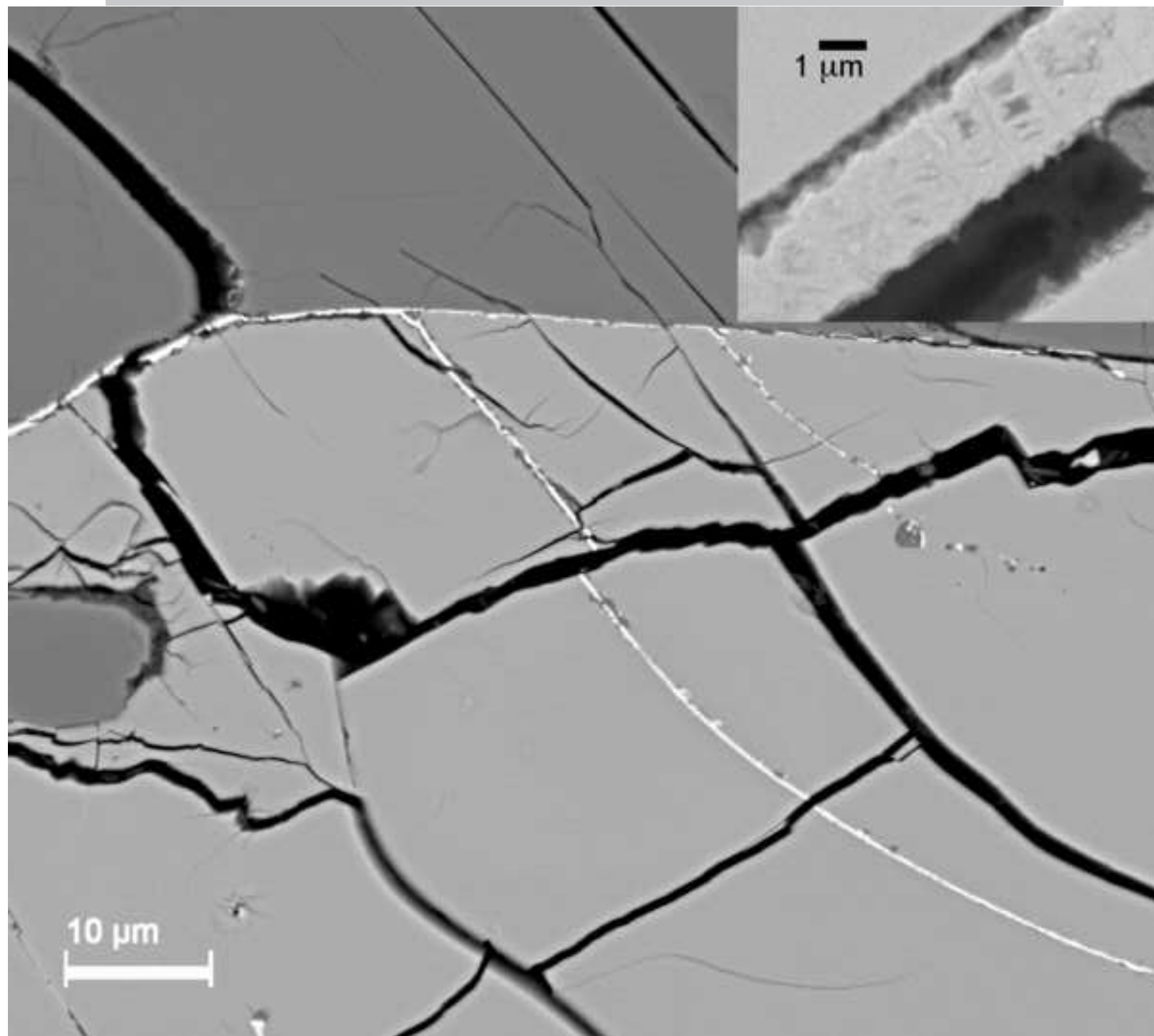


Figure 7

ACCEPTED MANUSCRIPT



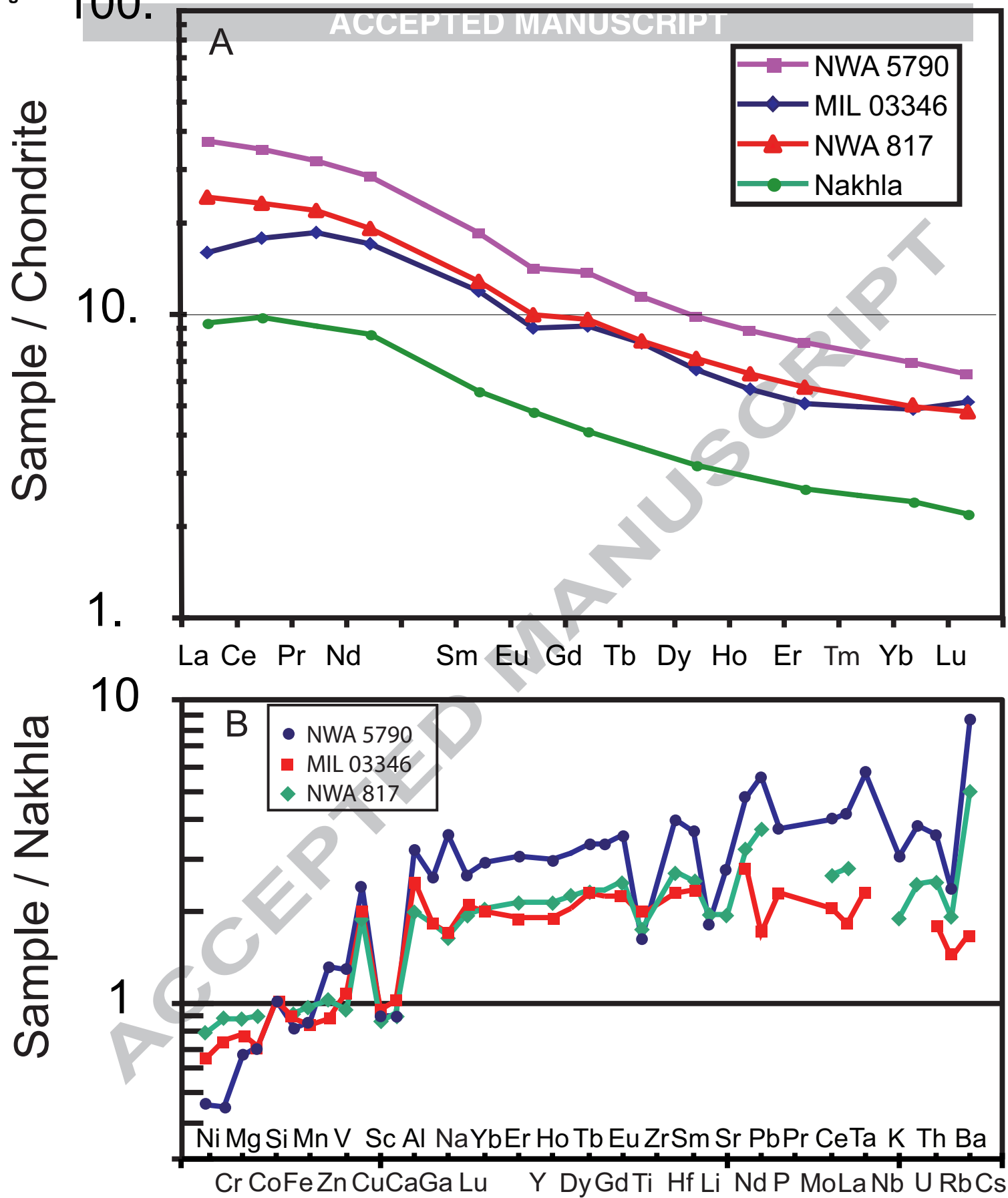


Figure 8 Jambon et al.

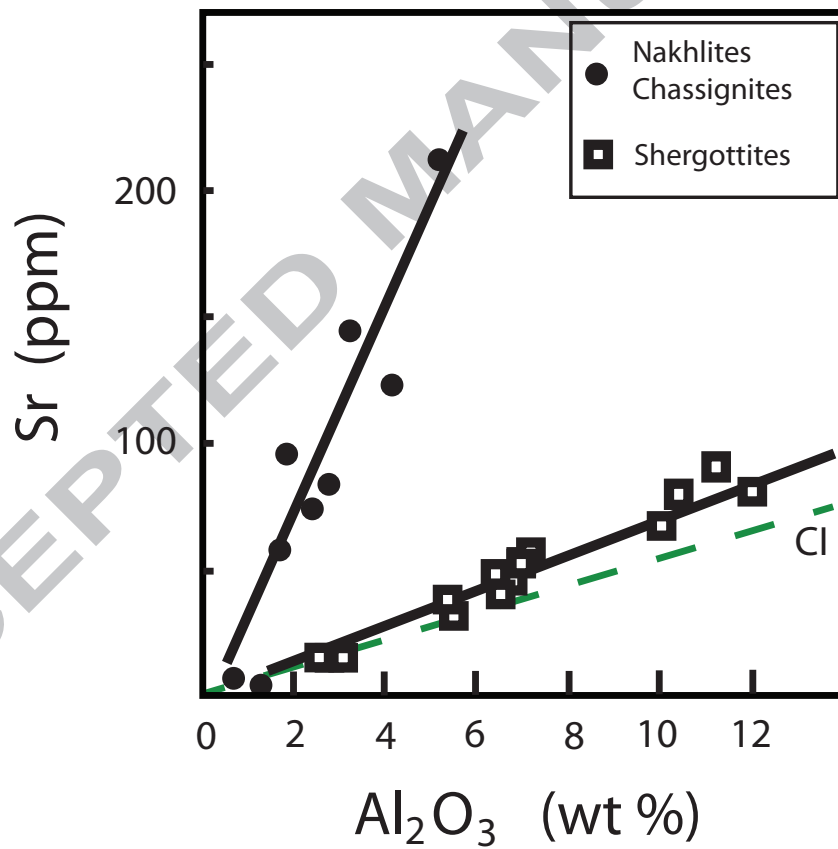


Figure 9. Jambon et al.

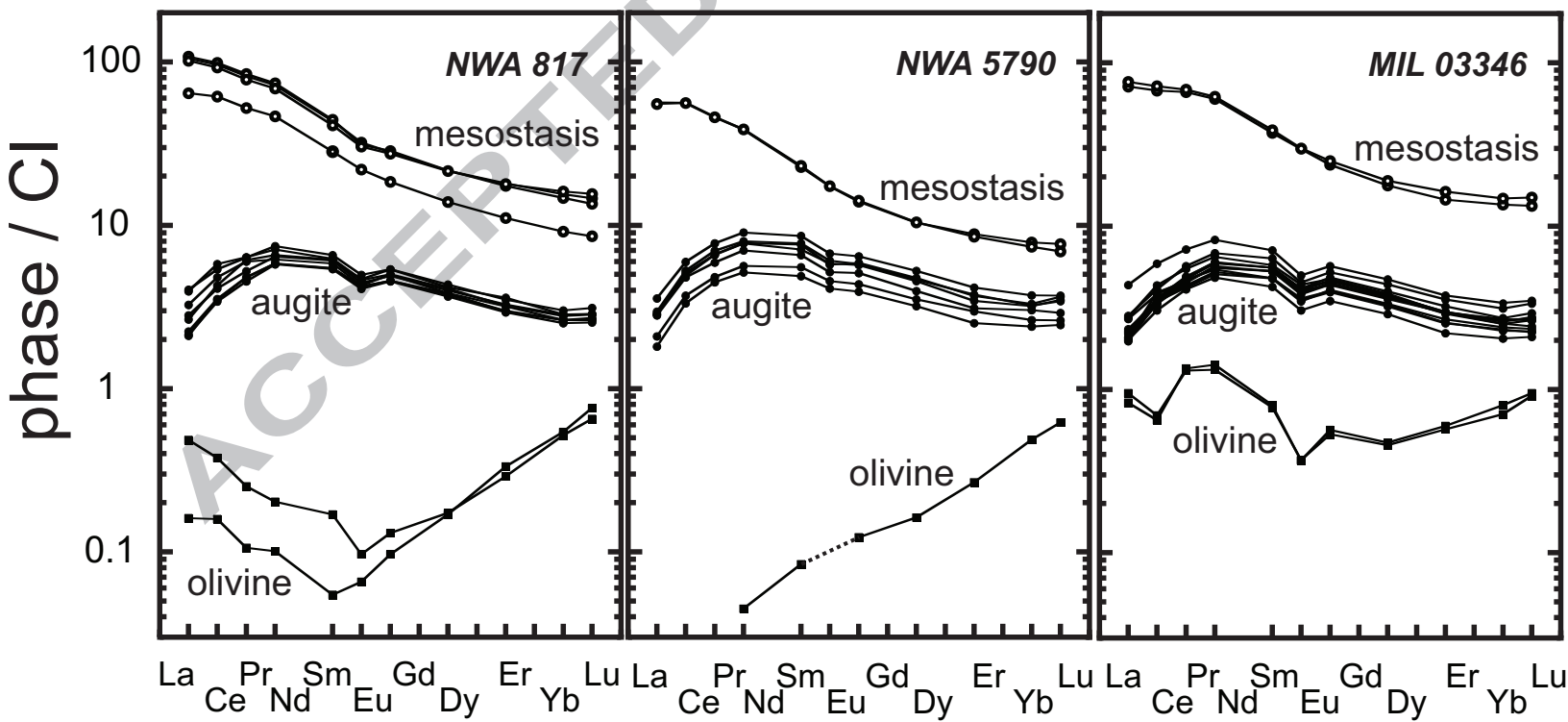


Figure 10: Jambon et al.

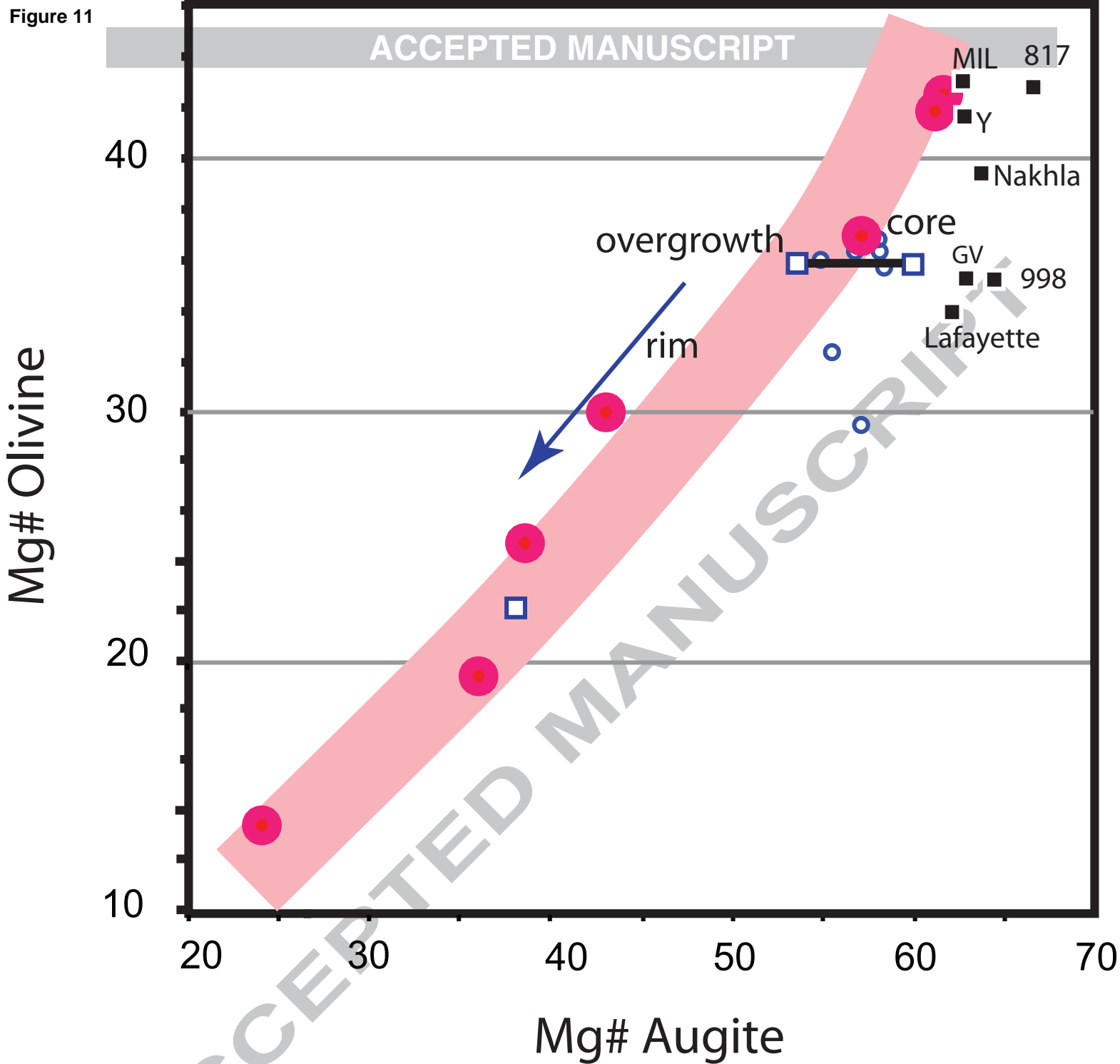


Figure 11: Jambon et al.

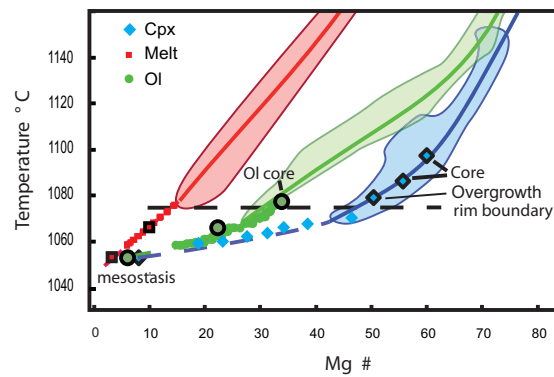
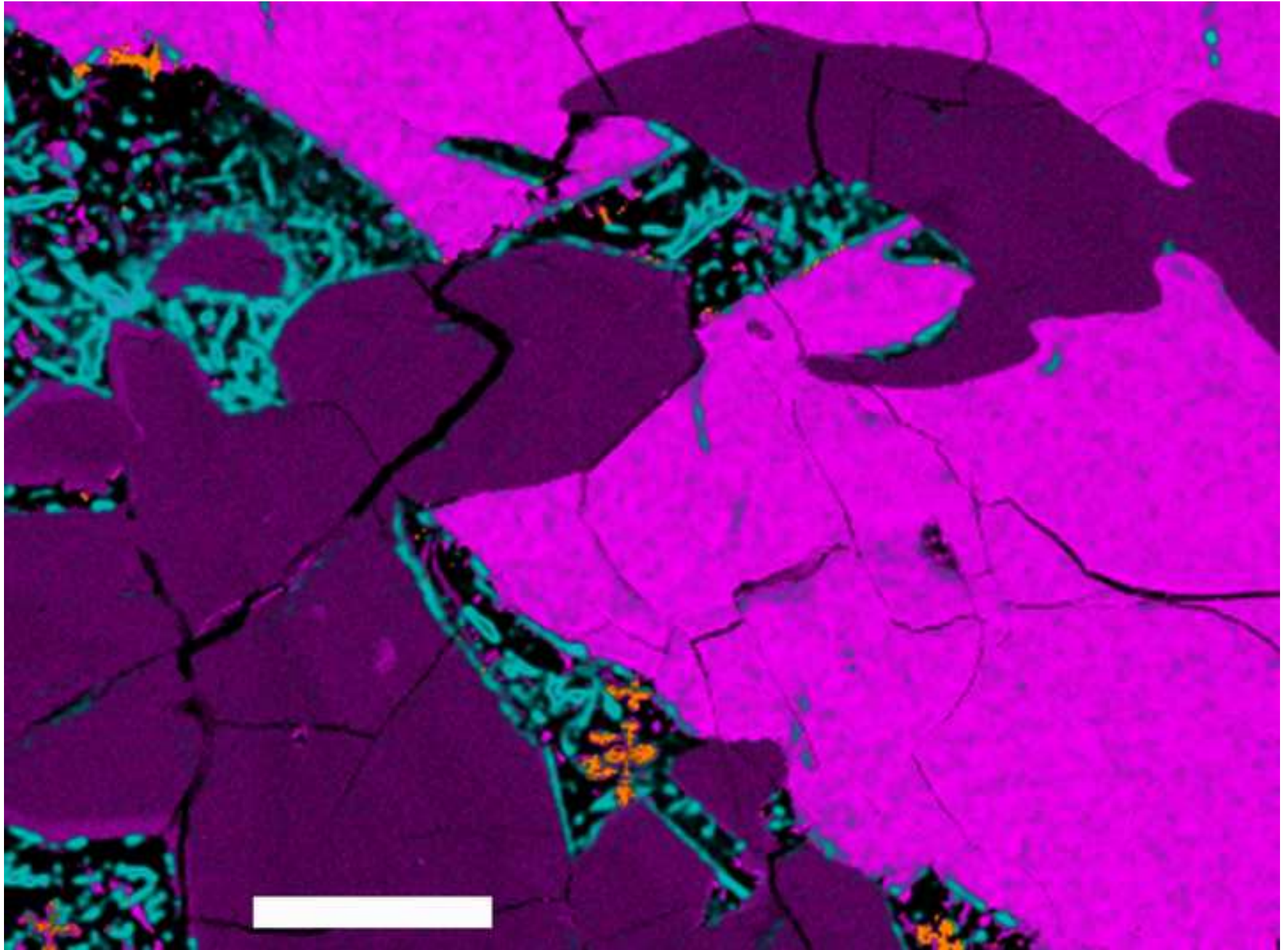
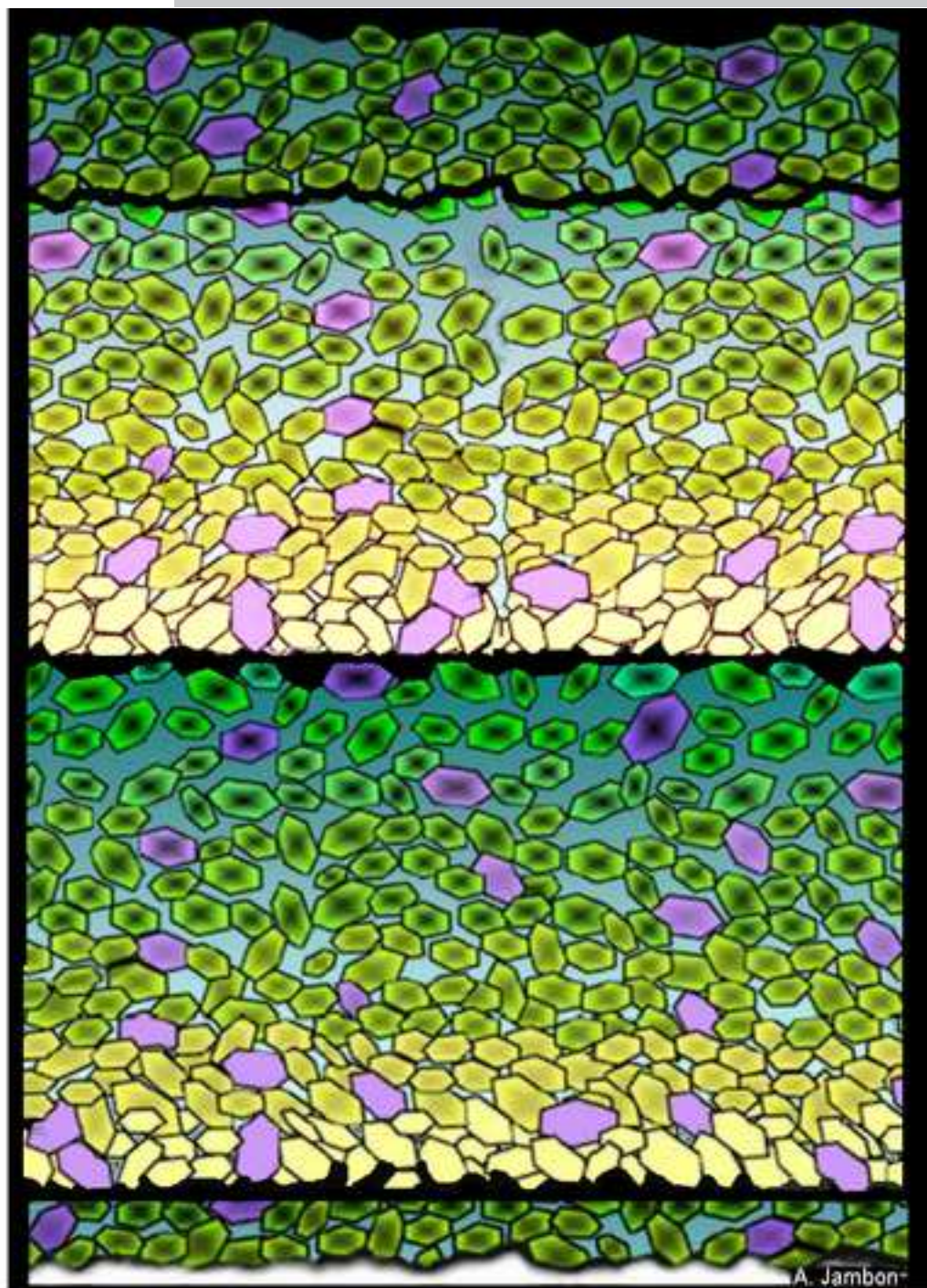


Figure 12. Jambon et al.

Figure 13
[Click here to download high resolution image](#)





Mg#	Augite	Olivine
MIL 03346	62.7	42.9
Y 000593	62.7	41.5
G Valadares Lafayette	62.9 62.9	34.8 33.9
Nakhla	62.5	39.3
NWA 817	66.5	42.4
NWA 998	64.5	35.2
NWA 5790	60	36

Iddingsite / Smectite

TABLES

Table 1 : Magnetic properties of nakhlites

Meteorite	Pf	T	$\log \chi$ $10^{-9} \text{ m}^3/\text{kg}$	% para	Ms Am^2/kg	n	mass g	ref
Governador Valadares	1.022	0.27	3.19	33.7	0.28	3	6.70	b,d
Lafayette	1.040		3.32	20.1	0.22	3	3.50	d
MIL03346	1.020	0.33	3.75	8.4	1.24	2	2.56	a,c
Nakhla	1.019	0.70	3.18	28.0	0.26	2	57.77	b
NWA 5790	1.005	0.52	3.81	6.2	1.19	1	1.16	a
NWA 817	1.019	-0.19	3.71	16.3	0.49	1	2.41	a
NWA 998	1.031	0.31	3.60	10.7	0.71	2	1.71	c
Yamato 000593*	1.027	0.30	3.56	14.1	0.66	4	1.34	a

% para = contribution of paramagnetic susceptibility to total susceptibility. References: a=this study; b=Gattacceca et al., (2008); c=Gattacceca et al., (2005); d=Collinson, (1997).

* Yamato 000593 has a different magnetic mineralogy compared to other nakhlites as it contains pyrrhottite in addition to titanomagnetite (Funaki et al., 2002).

Table 2: Representative analyses of augites

			core1	core2		Mesostasis					
			mean	mean	rim						
SiO ₂	50.77	51.10	50.83	51.19	50.68	49.36	47.75	45.96	45.28	45.79	46.72
TiO ₂	0.42	0.24	0.53	0.27	0.43	0.68	0.91	0.91	0.77	0.52	0.12
Al ₂ O ₃	1.03	0.86	1.34	0.85	1.29	1.77	2.40	3.10	2.49	0.86	1.89
Cr ₂ O ₃	0.21	0.33	0.18	0.32	0.21	0.06	0.02	0.06	0.00	0.08	0.06
MgO	11.32	11.99	10.47	12.04	10.68	9.45	7.93	5.61	5.51	4.11	1.32
FeO	15.37	14.86	16.25	14.55	15.96	19.38	22.42	26.19	28.27	27.57	28.82
MnO	0.47	0.43	0.49	0.43	0.45	0.51	0.64	0.63	0.72	0.62	0.54
CaO	19.47	19.01	19.12	18.98	19.19	17.35	16.26	15.06	13.84	17.62	16.52
Na ₂ O	0.37	0.35	0.36	0.30	0.34	0.40	0.42	0.50	0.28	0.17	0.49
K ₂ O	0.03	0.02	0.00	0.00	0.01	0.00	0.01	0.04	0.02	0.09	0.31
Total	99.48	99.28	99.66	99.00	99.29	98.96	98.77	98.10	97.22	97.53	96.87
Ti-Ts	0.01	0.01	0.02	0.01	0.01	0.02	0.03	0.03	0.02	0.02	0.00
Al-Ts	0.00	0.00	-0.02	0.00	0.00	0.00	0.02	0.04	0.06	0.05	0.00
Jd	0.03	0.03	0.03	0.02	0.03	0.03	0.03	0.04	0.02	0.01	0.04
En	0.32	0.34	0.30	0.35	0.31	0.28	0.23	0.17	0.17	0.13	0.04
Fs	0.24	0.23	0.26	0.23	0.25	0.31	0.36	0.43	0.43	0.40	0.49
Wo	0.39	0.39	0.40	0.39	0.39	0.36	0.33	0.30	0.27	0.36	0.38
Mg#	57	59	53	60	54	47	39	28	26	21	8
FeO/MnO	33	35	33	34	36	38	35	41	39	44	54

Table 3. Representative analyses of olivine

	Core				Rim			mesostasis
SiO ₂	32.68	32.25	32.63	33.29	31.66	31.79	32.42	29.93
TiO ₂	0.01	0.02	0.04	0.03	-	-	-	0.12
Al ₂ O ₃	bdl	0.04	bdl	bdl	0.11	0.02	0.02	0.1
Cr ₂ O ₃	bdl	0.03	0.06	0.03	0.00	-0.01	0.01	bdl
MgO	14.84	15.47	14.79	14.59	4.53	8.30	11.80	2.65
FeO	49.83	48.99	49.89	49.52	61.08	58.24	53.89	64.43
MnO	1.18	1.08	1.09	1.06	1.45	1.22	1.17	1.64
CaO	0.53	0.56	0.54	0.56	0.32	0.38	0.48	0.18
P ₂ O ₅	0.02	0.04	0.03	0.03	0.07	0.08	0.07	0.35
Total	99.14	98.51	99.13	99.11	99.03	99.94	99.76	99.45
Mg#	35	36	35	34	12	20	28	7
FeO/MnO	42	46	46	47	42	48	46	39

bdl: below detection limit

Table 4: Representative analyses of silicates in the mesostasis.

	plagioclase		K-spar	silica
SiO ₂	64.31	66.86	64.51	100.50
TiO ₂	0.04	0.34	-	0.01
Al ₂ O ₃	21.65	16.77	18.54	0.19
Cr ₂ O ₃	-	0.03	0.02	-
MgO	0.02	0.15	-	-
FeO	0.74	2.40	0.64	0.50
MnO	-	0.10	0.02	-
CaO	3.16	2.99	0.36	0.02
Na ₂ O	9.02	6.27	1.83	0.07
K ₂ O	1.14	1.70	13.36	0.05
P ₂ O ₅	0.05	0.56	0.06	-
Total	100.14	98.16	99.35	101.33
Si	2.85	3.12	2.99	
Al	1.13	0.92	1.01	
Fe	0.03	0.09	0.02	
Ca	0.15	0.15	0.02	
Na	0.78	0.57	0.16	
K	0.06	0.10	0.79	
An	0.15	0.18	0.02	
Ab	0.78	0.69	0.17	
Or	0.07	0.12	0.81	

Table 5: Nakhilites mesostase compositions compared, as measured in scanning mode.

	NWA 5790		MIL 03346		NWA 817	
n	12		13		53*	
	mean	error	mean	error	mean	error
SiO ₂	51.75	0.20	52.93	0.89	52.78	0.21
TiO ₂	1.03	0.01	0.82	0.14	0.82	0.02
Al ₂ O ₃	13.19	0.09	13.96	0.31	14.51	0.07
Cr ₂ O ₃	0.00	0.00	0.00	0.00	0.00	0.00
MgO	0.58	0.01	0.42	0.04	0.82	0.02
FeO	16.67	0.27	16.83	1.16	13.78	0.22
MnO	0.32	0.01	0.24	0.02	0.27	0.01
CaO	4.68	0.07	4.04	0.16	4.48	0.11
Na ₂ O	5.30	0.04	5.22	0.11	6.58	0.05
K ₂ O	1.62	0.02	1.06	0.05	2.10	0.03
P ₂ O ₅	1.04	0.05	0.84	0.03	1.58	0.05
SO ₂	-		-		0.18	0.03
Cl	-		-		0.11	0.00
Total	96.18	0.07	96.35	0.27	98.01	0.20
Mg#	5.8		4.3		9.6	

n is the number of scanned areas. Error is one standard deviation divided by $n^{1/2}$.

* areas scanned are four times smaller.

Table 6 : Representative analyses of alteration products in augite and olivine fractures compared to amphibiole from MIL 03346 (Sautter et al. 2006) and smectite in NWA 817 (Gillet et al. 2002) :

	Low Al		High Al		High Cl		MIL03346	NWA817	NWA817
n	42	42	14	14	5	5		16	25
	mean	sigma	mean	sigma	mean	sigma	M Inc. amphibole	mesost. smectite mean	olivine smectite mean
SiO ₂	46.61	2.21	49.89	7.14	44.56	5.99	37.48	46.51	42.82
TiO ₂	0.53	0.23	0.42	0.52	0.77	0.76	0.38	0.03	0.06
Al ₂ O ₃	2.42	1.31	15.08	3.42	13.43	2.43	8.62	2.26	0.21
MgO	7.92	2.08	0.89	0.59	0.83	0.18	0.97	7.56	5.69
FeO	18.69	3.30	12.18	6.92	18.10	5.46	31.95	28.42	36.45
MnO	0.49	0.10	0.19	0.13	0.19	0.07	0.36	0.28	0.55
CaO	16.79	1.55	7.71	3.08	7.96	1.13	9.23	0.14	0.25
Na ₂ O	0.43	0.26	3.55	1.41	2.85	1.28	0.76	0.06	0.18
K ₂ O	0.16	0.21	2.25	1.50	2.46	1.02	2.52	0.42	0.41
P ₂ O ₅	0.37	0.44	1.37	1.54	0.91	1.13	0.18	-	-
Cl	0.21	0.48	1.31	1.26	2.74	0.75	5.01	-	-
Total	94.74	1.18	94.88	2.93	94.86	4.97	97.78	85.68	86.65
Mg#	0.43		0.11		0.08		0.05	0.32	0.22
Si	7.21	0.20	7.11	0.54	6.66	0.39	5.97	7.37	7.04
Ti	0.06	0.03	0.04	0.06	0.09	0.09	0.05	0.00	0.01
Al	0.45	0.25	2.53	0.47	2.36	0.37	1.62	0.42	0.04
Mg	1.82	0.45	0.19	0.13	0.18	0.05	0.23	1.79	1.39
Fe	2.43	0.48	1.45	0.92	2.26	0.79	4.25	3.77	5.01
Mn	0.06	0.01	0.02	0.02	0.02	0.01	0.05	0.04	0.08
Ca	2.78	0.21	1.18	0.53	1.28	0.24	1.58	0.02	0.04
Na	0.13	0.08	0.98	0.34	0.83	0.32	0.23	0.02	0.06
K	0.03	0.04	0.41	0.26	0.47	0.16	0.51	0.09	0.09

Cl	0.06	0.13	0.32	0.33	0.69	0.23	1.35	-	-
----	------	------	------	------	------	------	------	---	---

Structural formulae calculated arbitrarily on the basis of 23 oxygen equivalent.

ACCEPTED MANUSCRIPT

Table 7: Representative analyses of oxides.

	Phenocrysts				Mesostasis			
SiO ₂	0.16	0.09	0.08	0.11	0.64	0.87	0.21	1.68
TiO ₂	10.32	10.94	12.11	11.12	19.63	20.83	22.38	24.73
Al ₂ O ₃	2.96	3.04	2.71	2.90	0.30	0.38	0.33	0.62
Cr ₂ O ₃	1.34	2.90	2.61	2.28	0.05	0.00	0.01	0.03
MgO	0.13	0.46	0.50	0.36	0.11	0.06	0.07	0.07
FeO	74.95	74.88	74.04	74.62	69.89	67.58	67.88	63.20
MnO	0.36	0.29	0.47	0.37	0.41	0.50	0.35	0.42
CaO	0.01	0.02	0.03	0.02	0.13	0.12	0.15	0.21
Na ₂ O	-	-	0.02	-	0.05	0.00	-	0.17
K ₂ O	0.01	0.00	0.01	0.01	0.04	0.04	0.01	0.09
SO ₂	0.01	0.00	0.01	0.00	0.03	0.00	0.00	0.07
P ₂ O ₅	-	0.01	-	0.00	0.00	-	-	0.04
NiO	-	0.02	0.04	0.02	0.00	-	-	0.03
Total	90.24	92.63	92.64	91.84	91.27	90.37	91.39	91.36
Si	0.01	0.00	0.00		0.03	0.04	0.01	0.07
Ti	0.31	0.32	0.35		0.59	0.63	0.67	0.74
Al	0.14	0.14	0.12		0.01	0.02	0.02	0.03
Cr	0.04	0.09	0.08		0.00	0.00	0.00	0.00
Mg	0.01	0.03	0.03		0.01	0.00	0.00	0.00
Fe	2.49	2.42	2.39		2.34	2.29	2.28	2.11
Mn	0.01	0.01	0.02		0.01	0.02	0.01	0.01
Fe ³⁺	1.19	1.13	1.09		0.77	0.65	0.62	0.38

Fe ²⁺	1.30	1.29	1.30	1.57	1.64	1.66	1.73
Fe ³⁺ /Fe	0.48	0.47	0.46	0.33	0.28	0.27	0.18
Ulvöspinel	0.31	0.32	0.35	0.59	0.63	0.67	0.74
Magnetite	0.59	0.56	0.55	0.38	0.33	0.31	0.19
Chromite	0.02	0.04	0.04	0.00	0.00	0.00	0.00
Spinel	0.07	0.07	0.06	0.01	0.01	0.01	0.01

Table 8 : Major (wt %) and trace (ppm) element composition of NWA 5790 and other nakhlites

	NWA 5790 a	MIL 03346 a	NWA 817 b	Nakhla c, d
SiO ₂	-	-	-	49.33
TiO ₂	0.57	0.69	0.61	0.35
Al ₂ O ₃	5.19	3.66	3.28	1.64
Cr ₂ O ₃	0.11	-	0.22	0.25
MgO	7.79	9.99	10.31	11.82
FeO	17.79	19.12	19.84	21.70
MnO	0.47	0.46	0.53	0.55
CaO	12.93	15.75	13.07	14.30
Na ₂ O	2.02	1.00	0.94	0.57
K ₂ O	0.52	0.27	0.32	0.17
P ₂ O ₅	0.37	0.25	-	0.10
Total	(47.76)	(51.19)	(49.12)	100.78
Mg#	44	48	48	49
Li	6.95	4.25	7.43	3.80
Be	0.60	0.30	0.44	-
Sc	49.9	54.5	47.0	55.0
V	243	208	181	192
Cr	769	1192	1519	1710
Co	38.5	35.7	49.0	54.0
Ni	41.0	49	71.0	90.0
Cu	16.24	8.2	12.70	6.70
Zn	90.73	61.3	71.52	70.0
Ga	9.57	6.51	6.77	3.70
Rb	7.39	4.14	6.06	3.15
Sr	210.6	132.0	145.0	75.0
Y	13.76	8.44	9.86	-
Zr	41.01	21.58	29.72	-
Nb	7.94	3.47	4.60	-

Mo	0.03	-	0.17	-
Cs	0.11	0.25	0.25	0.43
Ba	285.4	59.58	167.0	34.0
La	9.10	4.70	5.92	2.14
Ce	22.31	11.01	14.70	5.60
Pr	3.10	1.56	2.11	-
Nd	13.52	7.07	9.02	2.85
Sm	2.87	1.64	1.97	0.78
Eu	0.83	0.522	0.58	0.23
Gd	2.82	1.73	1.96	-
Tb	0.43	0.266	0.31	0.13
Dy	2.53	1.57	1.81	-
Ho	0.50	0.317	0.36	0.17
Er	1.34	0.851	0.95	-
Yb	1.15	0.766	0.82	0.40
Lu	0.16	0.114	0.12	0.06
Hf	1.17	0.72	0.78	0.29
Ta	0.51	0.20	0.25	0.09
W	0.80	0.33	0.45	0.18
Pb	2.82	0.91	1.90	0.51
Th	0.85	0.42	0.60	0.24
U	0.22	0.09	0.14	0.056

a: this work, b: Sautter et al. (2002), c: Dreibus et al. (1982), d: Nakamura et al. (1982)

Table 9: Trace element compositions of separate minerals in NWA 5790 as obtained by LA-ICP-MS.

	NWA 817 augite mean	MIL03346 augite mean	NWA5790 augite mean	NWA817 Olivine mean	MIL03346 Olivine mean	NWA5790 Olivine mean	NWA817 Mesostase mean	MIL03346 Mesostase mean	NWA5790 Mesostase mean
n	8	13	7	2	2	1	3	2	2
Ti	1823	1711	2200	119	121	269.19	-	4949	5 330
Co	35.9	37.5	42.5	103.7	124	171.1	-	8.9	11.6
Ni	63.7	63.2	57.4	173.8	195	224.6	-	1.8	3.3
Rb							24.47	11.88	14.66
Sr	39.0	33.2	38.8	2.12	0.25	-	541	481	282.3
Y	5.00	4.68	5.34	0.35	0.73	-	25.8	23.2	14.1
Zr	3.94	3.53	9.19	0.41	-	-	118	98	63.6
Ba	8.44	1.96	9.25	4.30	-	-	490	273	422
La	0.68	0.58	0.64	0.08	0.208	0.012	22.00	17.36	13.16
Ce	2.61	2.28	2.84	0.16	0.402	0.014	51.39	41.85	33.66
Pr	0.50	0.45	0.56	0.02	0.120	0.004	6.62	6.13	4.19
Nd	2.97	2.74	3.34	0.07	0.635	0.021	29.71	28.34	17.90
Sm	0.90	0.83	1.05	0.02	0.120	0.013	5.87	5.81	3.51
Eu	0.26	0.23	0.32	0.00	0.022	0.012	1.63	1.75	1.02
Gd	1.01	0.93	1.10	0.02	0.113	0.025	5.15	5.02	2.89
Dy	1.01	0.94	1.08	0.04	0.118	0.041	4.89	4.66	2.64
Er	0.53	0.49	0.56	0.05	0.097	0.044	2.64	2.55	1.44
Yb	0.46	0.44	0.52	0.09	0.127	0.082	2.32	2.38	1.28
Lu	0.07	0.07	0.08	0.02	0.023	0.015	0.32	0.35	0.18
Hf	0.18	0.15	0.21	0.01	-	-	2.83	2.74	1.62
Th	-	-	-	-	-	-	2.53	2.24	1.44
U	-	-	-	-	-	-	0.57	0.60	0.38

Table 10: Parent magma compositions

	J1	J2	J3	J4	NK01	S04	N	GH(6)	D
SiO ₂	52.54	52.33	52.40	52.12	49.8	51.2	49.01	55.4	45.13
TiO ₂	0.97	0.93	0.98	0.85	0.8	0.84	1.06	1.07	0.59
Al ₂ O ₃	11.69	11.03	11.68	9.24	7.5	7.1	2.85	9.4	3.39
Cr ₂ O ₃	0.02	0.03	0.01	0.04	0.1	nd	0.08	nd	0.31
MgO	1.72	2.32	1.70	4.39	4.6	4.6	5.22	4.9	12.06
FeO	18.71	18.81	19.09	17.98	22.3	19.6	26.23	13.4	26.84
MnO	0.36	0.36	0.36	0.35	0.5	0.53	0.73	0.24	0.88
CaO	6.70	7.38	6.64	9.54	10.4	11.2	13.92	10.2	10.57
Na ₂ O	4.61	4.31	4.57	3.50	1.1	2.1	0.97	3.2	0.86
K ₂ O	1.40	1.30	1.38	1.04	2.4	0.7	0.2	0.6	0.34
P ₂ O ₅	0.90	0.84	0.89	0.67	0.6	0.97	nd	nd	nd
Total	99.63	99.65	99.69	99.72	100.1	98.84	100.27	98.41	100.97
Mg#	14.1	18.0	13.7	30.4	27.0	29.6	26.2	33.3	44.5

J1-4 this work NWA 5790 : J1 before adcumulus growth, J2 before crystallization of Augite+olivine phenocrysts, J3 before dissolution of 6% of olivine xenocrysts, J4 melt in equilibrium with NWA 817 augite core.

NK01 Treiman and Goodrich (2001), S04: Stockstill et al. (2005), GH(6): Varela et al. (2001), N Longhi and Pan (1989), D Treiman (1986)